RSC Advances

PAPER

View Article Online
View Journal | View Issue



Cite this: *RSC Adv.*, 2023, **13**, 30753

# Pyrrolizine/indolizine-bearing (un)substituted isoindole moiety: design, synthesis, antiproliferative and MDR reversal activities, and *in silico* studies †

Amr L. AbdelSamad,[a] Mohammed T. El-Saadi,[bc] Ahmed M. Gouda[b] and Asmaa M. AboulMagd *[a]

Two new series of pyrrolizine/indolizine derivative-bearing (un)substituted isoindole moiety were designed and synthesized. The anticancer potential of the new compounds was evaluated against hepatocellular carcinoma (HepG-2), colorectal carcinoma, colon cancer (HCT-116), and breast cancer (MCF-7) cell lines. Compounds **6d** and **6o** were the most potent derivatives with $IC_{50}$ values ranging from 6.02 to 13.87 μM against HePG-2, HCT-116, and MCF-7 cell lines. Moreover, methyl analog of the fluoro-substituted indolizine derivative **6m** revealed significant antiproliferative activity against HePG-2, HCT-116, and MCF-7 cancer cell lines with $IC_{50}$ values of 11.97, 28.37, and 19.87 μM, respectively. The most active anticancer analogs, **6d**, **6m**, and **6o**, were inspected for their putative mechanism of action by estimating their epidermal growth factor receptor (EGFR) and cyclin-dependent kinase (CDK 2) inhibitory activities. Thus, compound **6o** displayed the most inhibitory activity against EGFR and CDK 2 with $IC_{50}$ values of 62 and 118 nM, respectively. Additionally, the quantitative real-time PCR analysis for the P-glycoprotein effect of compounds **6d**, **6m**, and **6o** was performed, in which compound **6o** illustrated significant down-regulation of P-gp against the HepG-2 cell line by 0.2732 fold. Mechanistic studies for the most active compounds involving the reversal doxorubicin (DOX) effect of compounds **6d**, **6m**, and **6o** were performed, which illustrated cytotoxic activity with $IC_{50}$ 22.27, 3.88, and 8.79 μM, respectively. Moreover, the apoptotic activity of the most active derivative **6o** on HCT-116 cancer cells showed accumulation in the G1 and S phases of the cell cycle.

Received 5th August 2023
Accepted 8th October 2023

DOI: 10.1039/d3ra05310e

rsc.li/rsc-advances



## 1. Introduction

Cancer is one of the most prevalent conditions affecting public health, and it is the second-leading cause of mortality after cardiovascular diseases.[1] The clinical efficacy of anticancer drugs that are currently in use has decreased, which may be attributed to certain factors such as increased drug resistance, establishment of tumor resistance, and the severe adverse effects of chemotherapeutic agents.[2,3] In addition, multi-drug resistance of cancerous tumors is one of the primary factors contributing to the clinical progression of these tumors.[4,5] Although targeted medications and immunotherapy for cancer are becoming common, there is still an urgent need to develop more effective and less resistant anticancer agents.[6,7]

Overexpression of ATP-binding cassette (ABC) transporters is a common cause of multi-drug resistance (MDR), which is the leading cause of chemotherapy failure.[8] ABC transporters have been researched extensively; those related to MDR in cancer cells include ABCB1, ABCC1, and ABCG2. ABCB1, often referred to as P-glycoprotein (P-gp), has a high expression in several vital organs, such as the liver, kidney, lung, placenta, and intestines, for the purposes of protection and detoxification.[9,10] According to the literature, verapamil (**I**), febuxostat (**II**), and the aminopyrimidine-based drug (**III**) exhibit potential P-glycoprotein inhibitory activity (Fig. 1).[11–13]

Recent studies showed that isoindole derivatives might be potential anticancer agents. For example, compound (**IV**) exhibited good activity against A549 lung cancer cell lines at $IC_{50} = 19$ μM when compared to 5-fluorouracil (**V**) with $IC_{50} < 5$ μM.[14] Moreover, derivative (**VI**) showed significant activity against S1-B1-20 cell lines with $IC_{50} = 0.81$ μM; interestingly, the latter derivative was designed as an MDR reversal agent, which showed promising findings, and the mechanism of action of

[a]*Department of Pharmaceutical Chemistry, Faculty of Pharmacy, Nahda University in Beni-Suef (NUB), Beni-Suef 62513, Egypt. E-mail: asmaa.aboulmaged@nub.edu.eg*
[b]*Department of Pharmaceutical Chemistry, Faculty of Pharmacy, Beni-Suef University, Beni-Suef 62514, Egypt*
[c]*Department of Pharmaceutical Chemistry, Faculty of Pharmacy, Sinai University-Kantra Branch, Ismailia, Egypt*

† Electronic supplementary information (ESI) available. See DOI: https://doi.org/10.1039/d3ra05310e

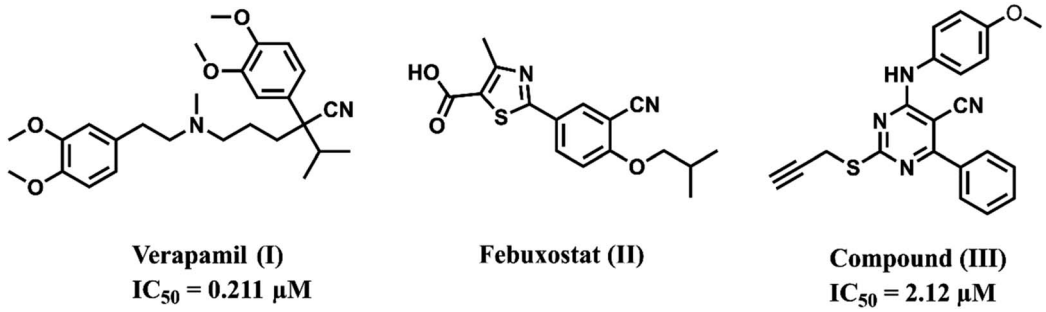


Fig. 1 Examples of compounds showing P-glycoprotein inhibitory activity.

this compound is believed to involve down regulation of the drug efflux pump, P-glycoprotein.[15] Furthermore (**VII**), produced a potentiation effect in the MDR cell line in combination with VIN (60.0%) and PTX (80.5%) (Fig. 2).[16]

From another point of view, the pyrrolizine ring comprises the basic skeleton in some compounds with diverse pharmacological activities such as antiviral, antimicrobial, anti-inflammatory, and anticancer activities. It was reported that pyrrolizine-based compounds have the ability to exhibit antitumor activities as a result of their ability to cross-link DNA.[17–19] Interestingly, licofelone (**VIII**) is a pyrrolizine-based compound that exhibited significant cytotoxic activity with an $IC_{50}$ value of 5.5 μM on breast cancer cell line (MCF-7) by indirect blocking of the EGFR kinase.[20–22] In addition, MR22388 (**IX**) exhibited notable anticancer activity against leukemia L1210 cells, with an $IC_{50}$ value of 15 nM.[23] Pyrrolizine-containing compounds have been reported to show potent inhibition of the mitogen-activated protein kinase (MAP)

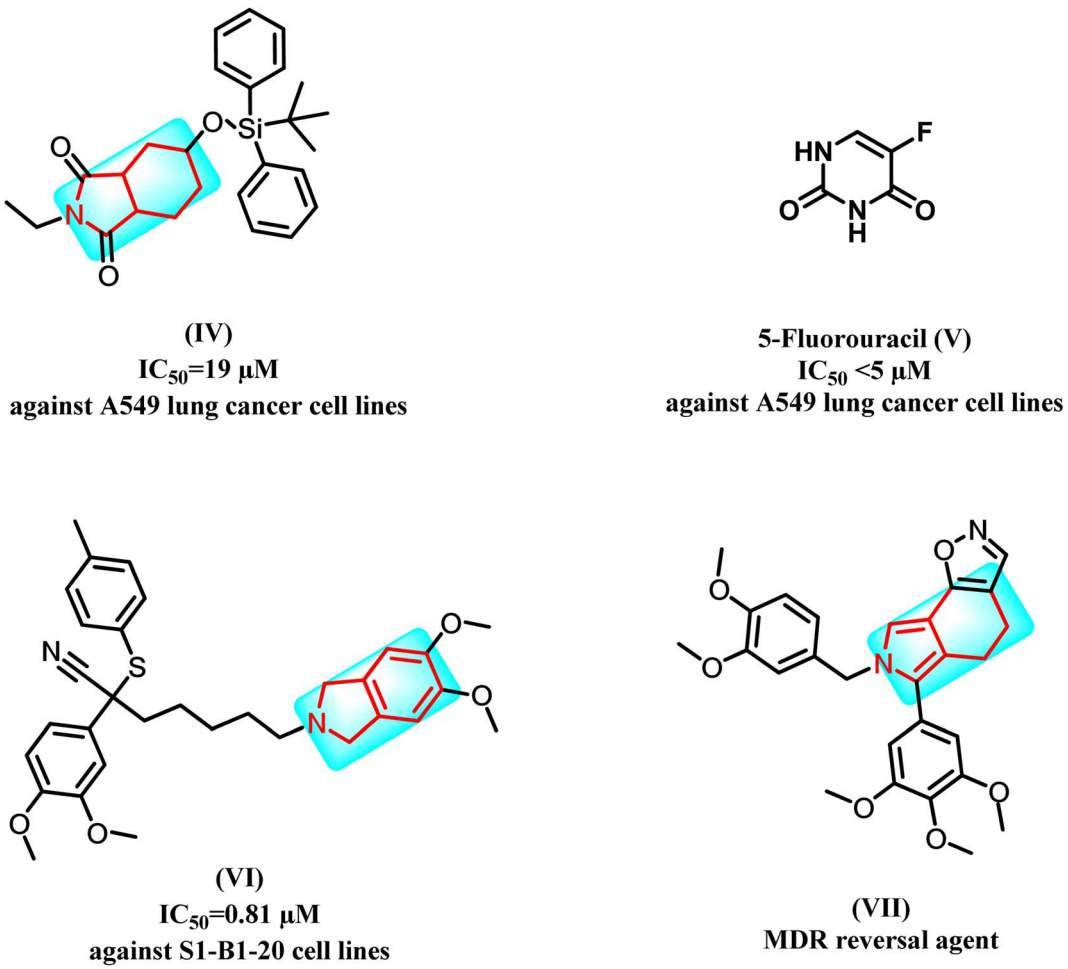


Fig. 2 Examples of anticancer agents bearing isoindole moiety.

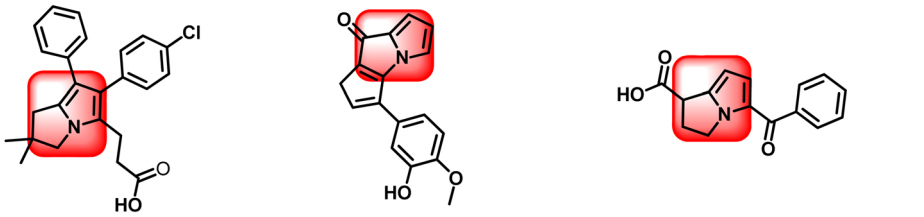


Fig. 3 Pyrrolizine-based compounds as anticancer agents.

pathway regulated by the conserved receptor tyrosine kinase (EGFR/MAPK) signaling mechanism. Thus, these compounds displayed strong inhibition of several protein kinases, mainly EGFR and CDK-2, in addition to their ability to inhibit tubulin polymerization, which allowed it to trigger apoptosis in leukemia cell lines (Fig. 3).[24,25]

Also, Ketorolac (**X**), another drug based on pyrrolizine, had significant anticancer activity against lung cancer cell lines A549 with an $IC_{50}$ value of about 13 μM[26] (Fig. 3).[27]

Modern bio-/chemoinformatics methods can effectively support the estimation of the most likely targets for small compounds. Thus, the SwissTarget web tool makes predictions about the likeliest protein targets for our designed compounds, resulting in high predictions towards kinase proteins.[28] So, this encouraged us to target kinase proteins as epidermal growth factor receptor tyrosine kinases (EGFR TKs) and cyclin-dependent kinases (CDKs) due to their wide carcinogenic signaling pathways.[29]

Increasing levels of epidermal growth factor receptor EGFR and its endogenous ligands (EGF) have been shown to be a keystone in carcinogenesis as well as playing the most important role in cancer growth.[30] Therefore, EGFR is regarded as an applicable target for the improvement of novel anticancer drugs. According to the literature, several pyrrolizine derivatives were developed and synthesized with the belief of more binding moieties, following the pharmacophoric features of EGFR TKIs overcoming the multi-resistance that may have emerged. For example, compound (**XI**) exhibited EGFR TK percent inhibition of 97.6% at 10 μM and showed anti-proliferative activity against MCF-7 breast cancer cell lines with $IC_{50}$ value 8.6 μM (Fig. 4).[31]

In the same context, cell cycle progression and cellular proliferation are both regulated by a family of enzymes known as cyclin-dependent kinases (CDKs).[32] They act by phosphorylating crucial serine and threonine residues in host proteins, allowing those proteins to be activated.[32] It is widely accepted that blocking CDKs could aid in preventing the unchecked cellular growth observed in some cancers.[33]

Recent research studies have demonstrated that pyrrolizine scaffold can also participate in designing anticancer agents *via* inhibition of CDK-2 enzyme. Compounds (**XII**) and (**XIII**) showed inhibition of CDK-2 enzyme at $IC_{50}$ of 0.63 μM and 0.025 μM, respectively.[34,35] (Fig. 4).[36]

Recently, a novel form of cancer treatment called multi-target anticancer drugs has surfaced.[37] This method garnered a lot of

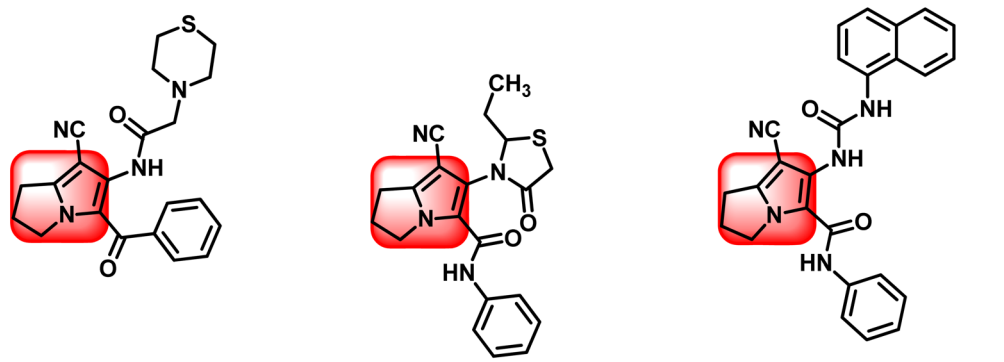


Fig. 4 Pyrrolizine as EGFR TK and CDK-2 inhibitors.

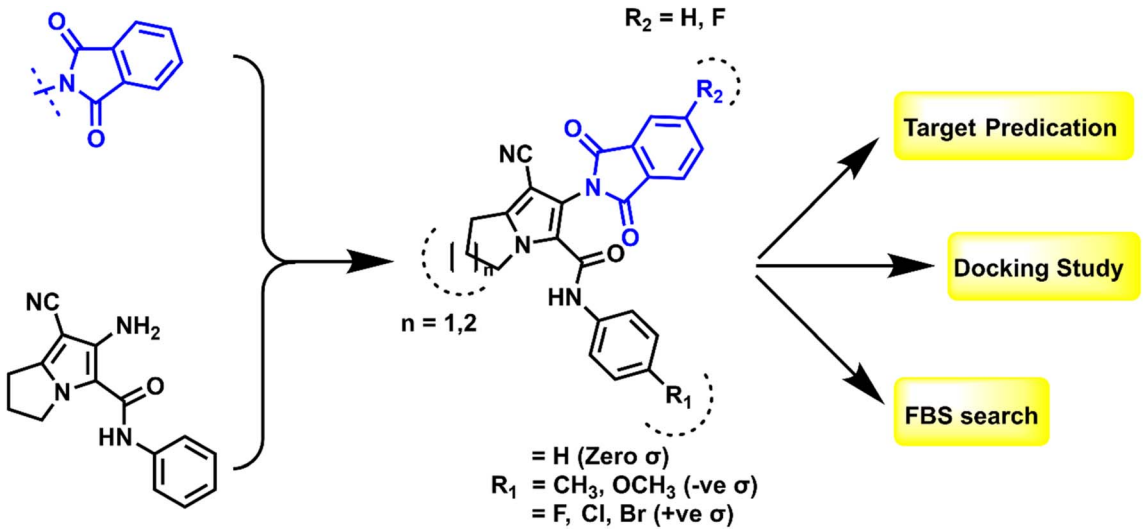


Fig. 5 Rationale design of the final compounds **6a–q**.

interest since it might offer a better alternative for combination therapy with less toxicity and drug–drug interaction issues.[38] Literature has many examples of multi-target molecules, such as EGFR/CDK-2 dual inhibitors as potent anticancer agents.[36,39,40]

### 1.1. Design and rationale

Based on the findings that we retrieved from the literature, hybridization between isoindoline nucleus and pyrrolizine moiety could serve as good anti-proliferative agents *via* dual inhibition to EGFR TK and CDK-2.[41,42] The shared pharmacophoric binding moieties include: (a) hybrid isoindoline-pyrrolizine moiety acts as main scaffold providing the ATP binding site moiety; (b) cyano group may form strong binding interactions with the key amino acids at the active domains of EGFR TK or CDK-2 enzymes and also, considered as an important pharmacophore among P-glycoprotein inhibitors against MDR cancer cell lines; and (c) one or two amide linker between the pyrrolizine main scaffold and the hydrophobic tail I. Regarding the above-mentioned pharmacophore, the newly synthesized compounds were designed as EGFR TK and CDK-2 dual inhibitors by maintaining the essential moieties and applying some lead optimization strategies, which can be summarized in (a) substitution on the hydrophobic tail (phenyl ring) with small and large lipophilic groups with electron donating and electron withdrawing properties to evaluate the structure–activity relationship of this position; (b) ring expansion of pyrrolizine ring to indolizine to assess its possible effect on the anti-proliferative activity, all shown at Fig. 5. The synthesized compounds were confirmed by different spectroscopic techniques to ensure their chemical structures and purity. All the compounds were evaluated for the anti-proliferative activity against HePG2 liver cancer, HCT-116 colon cancer, and MCF-7 breast cancer cell lines. Then, the effect of the most potent compounds on EGFR TK and CDK-2 was also evaluated. Additionally, the most active compounds were tested for their activity against MDR cancer cell lines.

Furthermore, the promising candidates were subjected to apoptosis assay and cell cycle analysis to determine their apoptotic mechanism. Finally, *in silico* study was performed to elucidate the binding of the active compounds inside their active sites.

## 2. Results and discussion

### 2.1. Chemistry

The designed compounds were synthesized according to the chemical pathway outlined in Scheme 1. A literature survey showed that the acetanilide derivatives **2a–f** were obtained through acylation of the appropriate amines with chloroacetyl chloride using different reaction conditions such as triethylamine, potassium carbonate, sodium acetate or pyridine in different solvents such as glacial acetic acid, dichloromethane, DMF or acetone.[43–46] In this study, the acetanilide derivatives **2a–f** were synthesized with good yield using acetic acid and sodium acetate according to the method by Kumar *et al.*[47] On the other hand, intermediates **4a and b** were synthesized by reacting 2-pyrrolidinone **3a** or 2-piperidinone **3b** with malononitrile in dry benzene *via* condensation reaction.[48] These intermediates were confirmed by their melting points, as reported. In this work, two series of the target compounds were obtained *via* the reaction of intermediates **4a and b** with the appropriate anilides **2a–f** in acetone catalyzed by potassium carbonate to afford the corresponding key intermediates pyrrolizine derivatives **5a–f** or indolizine derivatives **5g–j**, respectively.[48] The reported intermediates, pyrrolizine derivatives **5a–f** and indolizine derivatives **5g and h**, were confirmed by their reported melting points and different spectral data according to the literature.[27,48] However, two newly synthesized indolizine derivatives **5i** and **5j** were synthesized and confirmed by different spectroscopic techniques. IR spectra of the latter compounds **5i** and **5j** revealed absorption bands in the range of 3210–3320 $cm^{-1}$ (forked band), indicating the presence of $-NH_2$

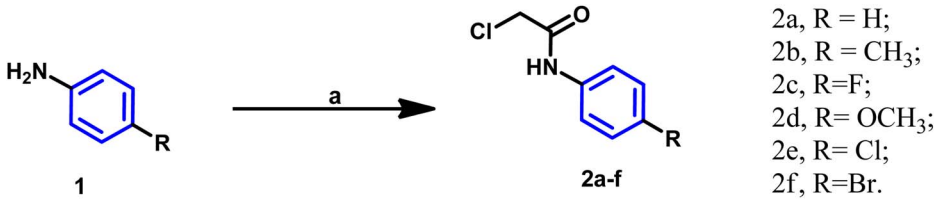


2a, R = H;
2b, R = $CH_3$;
2c, R=F;
2d, R= $OCH_3$;
2e, R= Cl;
2f, R=Br.

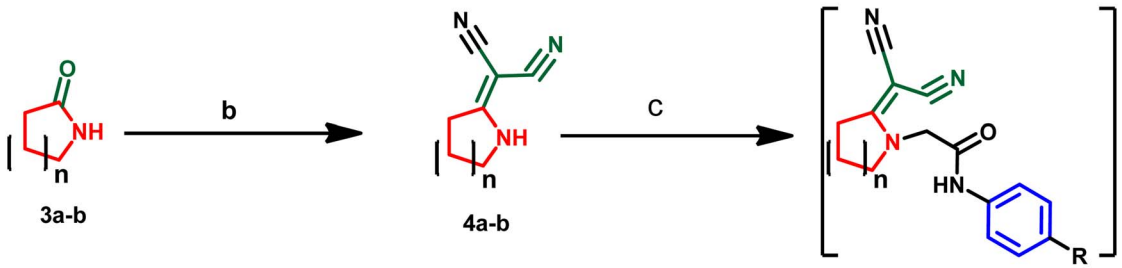


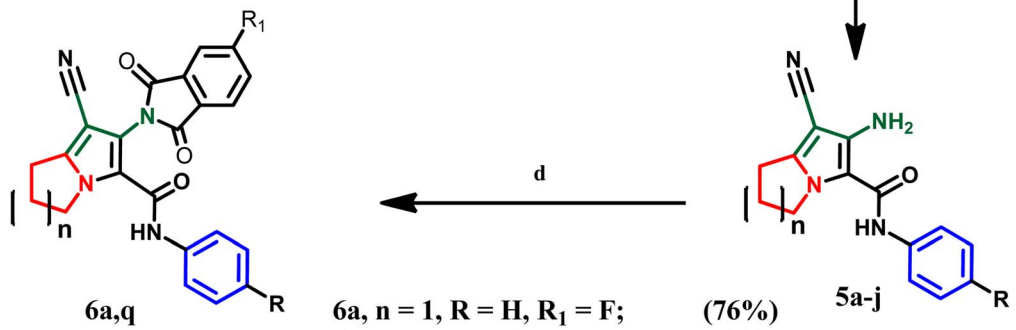


**6a, n = 1, R = H, $R_1$ = F; (76%)**
**6b, n = 1, R = $CH_3$, $R_1$ = F; (73%)**
**6c, n = 1, R = F, $R_1$ = H; (67%)**
**6d, n = 1, R = F, $R_1$ = F; (79%)**
**6e, n = 1, R = $OCH_3$, $R_1$ = H ; (72%)**
**6f, n = 1, R = $OCH_3$, $R_1$ = F ; (74%)**
**6g, n = 1, R = Cl, $R_1$ = F; (77%)**
**6h, n = 1, R = Br, $R_1$ = H; (66%)**
**6i, n = 1, R = Br, $R_1$ = F; (71%)**
**6j, n = 2, R = H, $R_1$ = H; (81%)**
**6k, n = 2, R = H, $R_1$ = F; (85%)**
**6l, n = 2, R = $CH_3$, $R_1$ = H; (83%)**
**6m, n = 2, R = $CH_3$, $R_1$ = F; (86%)**
**6n, n = 2, R =F, $R_1$ = H ; (85%)**
**6o, n = 2, R = F, $R_1$ = F ; (80%)**
**6p, n = 2, R =$OCH_3$, $R_1$ = H; (87%)**
**6q, n = 2, R =$OCH_3$, $R_1$ = F . (82%)**

**5a, n=1, R=H;**
**5b, n=1, R=$CH_3$;**
**5c, n=1, R=F;**
**5d, n=1, R=$OCH_3$;**
**5e, n=1, R=Cl;**
**5f, n=1, R=Br;**
**5g, n=2, R=H;**
**5h, n=2, R=$CH_3$;**
**5i, n=2, R=F;**
**5j, n=2, R=$OCH_3$.**

Scheme 1 Synthesis pathway of the final compounds **6a–q**. Reagents and conditions: (a) $ClCH_2COCl$, acetic acid, $CH_3COONa$, stirring, 1 h; (b) $(CH_3O)_2SO_2$, dry benzene, $CH_2(CN)_2$, reflux, 8 h; (c) compounds **2a–f**, acetone, $K_2CO_3$, reflux, 24 h; (d) un/substituted phthalic anhydride, glacial acetic acid, reflux, 4–6 h.

(primary amine). Also, other absorption bands in the range of 2212–2215 $cm^{-1}$ were assigned to the cyano group and stretching bands in the range of 1665–1675 $cm^{-1}$ were attributed to the amidic carbonyl group. Moreover, the $^1$H NMR spectrum of these compounds revealed four signals in the range of $\delta$ 2.51–4.23 ppm, attributed to the aliphatic methylene groups of indolizine nucleus as well as a singlet signal at $\delta$ 5.24–5.76 ppm assigned to amino ($-NH_2$) group. In addition to the appearance of two doublets of doublet signals at the aromatic range assigned to four aromatic protons of *para*-substituted phenyl ring and the appearance of singlet signal at $\delta$ 9.97–10.20 ppm indicating the –NH– of the amidic moiety. Furthermore, the intermediate **5j** was characterized by the appearance of a singlet signal at $\delta$ 3.79 ppm, attributed to three aliphatic protons of the methoxy group ($-OCH_3$). Finally, the target compounds **6a–q** were obtained *via* condensation of intermediates **5a–j** with phthalic anhydride or 4-fluoro phthalic anhydride using glacial acetic acid as a dehydrating agent and solvent. These compounds were confirmed by several spectroscopic methods. IR spectra of the mentioned compounds revealed the disappearance of the forked peak assigned to $-NH_2$ of the intermediates, and the appearance of additional intense peaks between 1697 and 1778 $cm^{-1}$ attributed to two carbonyl groups of the isoindolin-1,3-dione moiety as well as, sharp absorption bands at 2210–2237 $cm^{-1}$, indicating the cyano group. Moreover, absorption bands at 2910–2960 $cm^{-1}$ and 3030–3070 $cm^{-1}$ were assigned to aliphatic (–C–H) and aromatic (=C–H), respectively. Additionally, sharp absorption bands at 3282–3329 $cm^{-1}$ indicate the –NH of the amidic group. Also, $^1$H-NMR spectrum of compounds **6a–i** revealed three signals in the range of $\delta$ 1.92–4.39 ppm, attributed to the aliphatic methylene groups of the pyrrolizine ring, while the $^1$H-NMR spectrum of compounds **6j–q** showed four signals in the range of $\delta$ 1.86–4.23 ppm assigned to indolizine nucleus. The $^1$H-NMR spectrum of compounds **6a–q** showed the disappearance of the $-NH_2$ signal and increasing intensity of aromatic proton at the aromatic range $\delta$ 6.57–8.12 ppm due to additional phenyl moiety, in addition to a singlet signal at the range of $\delta$ 9.10–9.99 ppm assigned to amidic –NH– which was exchanged with $D_2O$. Moreover, all synthesized compounds were confirmed by $^{13}$C-NMR, which revealed three signals in the range of $\delta$ 165.02–167.88 ppm, indicating the carbonyl carbons of each derivative. Additionally, a distinctive signal at $\delta$ 117.3–120.2 was attributed to the carbon of the cyano group. Moreover, derivatives **6a–i** showed three signals in the range of $\delta$ 25.2–49.4 ppm, attributed to the aliphatic carbons of the pyrrolizine ring, while derivatives **6j–q** showed four signals in the range of $\delta$ 20.3–47.6 ppm. Finally, mass spectroscopy revealed the molecular mass of each compound in *m*/*z*.

## 2.2. Biological evaluation

**2.2.1. Cytotoxic activity against liver (HePG2), colon (HCT-116), and breast (MCF-7) cancer cell lines.** Evaluation of the anticancer activity was performed against three cancer cell lines, namely liver (HePG2), colon (HCT-116), and breast (MCF-7) cancer cell lines. Whereas doxorubicin (DOX) was used as a positive control,[49] as shown in Table 1. The survival curve was obtained by plotting concentrations of the compound under

Table 1 Cytotoxic activity of compounds against HePG2, HCT-116, and MCF-7 tumor cell lines

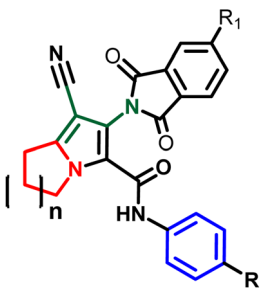


*In vitro* cytotoxicity $IC_{50}$ (μM)

| Compound No | Substitution | | | | | | Compound no | Substitution | | | | | |
|---|---|---|---|---|---|---|---|---|---|---|---|---|---|
| | *n* | R | $R_1$ | HePG2 | HCT-116 | MCF-7 | | *n* | R | $R_1$ | HePG2 | HCT-116 | MCF-7 |
| DOX[a] | — | — | — | 4.50 ± 0.2 | 5.23 ± 0.3 | 4.17 ± 0.2 | **6i** | 1 | Br | F | 20.44 ± 1.5 | 14.27 ± 1.1 | 25.32 ± 2.0 |
| **6a** | 1 | H | F | 85.14 ± 4.1 | >100 | 93.55 ± 4.7 | **6j** | 2 | H | H | 34.13 ± 1.9 | 22.09 ± 1.6 | 31.26 ± 2.3 |
| **6b** | 1 | $CH_3$ | F | 55.38 ± 3.2 | 66.33 ± 3.1 | 58.11 ± 3.3 | **6k** | 2 | H | F | 78.24 ± 3.8 | 83.65 ± 4.0 | 80.62 ± 4.1 |
| **6c** | 1 | F | H | 49.08 ± 2.9 | 47.87 ± 2.6 | 54.65 ± 3.1 | **6l** | 2 | $CH_3$ | H | 61.62 ± 3.5 | 57.51 ± 3.1 | 63.22 ± 3.5 |
| **6d** | 1 | F | **F** | **7.97 ± 0.5** | **9.49 ± 0.6** | **13.87 ± 0.9** | **6m** | **2** | **$CH_3$** | **F** | **11.97 ± 0.8** | **28.37 ± 1.9** | **19.87 ± 1.4** |
| **6e** | 1 | $OCH_3$ | H | 45.38 ± 2.5 | 38.14 ± 2.4 | 42.71 ± 2.5 | **6n** | 2 | F | H | 65.44 ± 3.7 | 71.27 ± 3.5 | 75.84 ± 3.9 |
| **6f** | 1 | $OCH_3$ | F | 88.31 ± 4.3 | >100 | >100 | **6o** | **2** | **F** | **F** | **6.02 ± 0.3** | **5.84 ± 0.2** | **8.89 ± 0.5** |
| **6g** | 1 | Cl | F | 52.04 ± 2.8 | 60.19 ± 3.3 | 69.44 ± 3.7 | **6p** | 2 | $OCH_3$ | H | 73.33 ± 3.9 | 79.63 ± 3.7 | 86.89 ± 4.3 |
| **6h** | 1 | Br | H | 91.36 ± 4.8 | >100 | >100 | **6q** | 2 | $OCH_3$ | F | 41.20 ± 2.3 | 32.19 ± 2.2 | 37.44 ± 2.6 |

[a] DOX: Doxorubicin.

investigation against the survival fraction of the tumor cells. Then, results were expressed in half maximal inhibitory concentration ($IC_{50}$). A closer look at the results regarding the pyrrolizine series against the three cancer cell lines revealed that the difluoro substituted derivative **6d** was the most potent compound, with $IC_{50}$ values of 7.97, 9.49, and 13.87 μM against HePG2, HCT-116, and MCF-7, respectively. Regarding the indolizine series, the difluoro substituted derivative **6o** exhibited the most anti-proliferative activity, with $IC_{50}$ values of 6.02, 5.84, and 8.89 μM against HePG2, HCT-116, and MCF-7, respectively. Additionally, methyl analogue of the fluoro-substituted indolizine derivative **6m** revealed significant anti-proliferative activity against HePG2, HCT-116, and MCF-7 cancer cell lines with $IC_{50}$ values of 11.97, 28.37, and 19.87 μM, respectively. Unfortunately, other pyrrolizine and indolizine derivatives showed moderate to weak activity against the three cell lines with $IC_{50}$ values between 20.44 and 91.36 μM against the HePG2 cell line, 22.09 to >100 μM against HCT-116, and 25.32 to >100 μM against MCF-7.

The relationship between cytotoxic activity and the structure of the synthesized compounds revealed that the substitution of the isoindolinedione moiety with a fluoro group remarkably showed higher anti-proliferative activity than the unsubstituted isoindolinedione moiety in all pyrrolizine and indolizine derivatives. As well as, substitution with a small electron withdrawing group, such as fluoro atom on the phenyl ring in pyrrolizine and indolizine derivatives, increases the cytotoxic activity against the three cancer cell lines. Also, methylphenyl or bromophenyl with fluoroisoindolinedione series showed potent anti-proliferative activity, unlike the remaining tested derivatives chloro, methoxy, and the unsubstituted derivatives. Finally, the ring expansion of the pyrrolizine ring to the indolizine ring significantly decreased the anti-proliferative activity of the tested compounds.

#### 2.2.2. Enzyme inhibition activity

*2.2.2.1 EGFR inhibition assay.* Depending on the anti-proliferative screening of the synthesized compounds, the most active compounds **6o**, **6d**, and **6m** were subjected to epidermal growth factor activity.[36] The results revealed that the difluoro indolizine derivative (**6o**) showed the most inhibitory activity against the EGFR enzyme with an $IC_{50}$ value of 62 nM in comparison to the positive control lapatinib ($IC_{50}$ = 69 nM). Also, methylphenyl fluoroisoindolinedione derivative (**6m**) and difluoropyrrolizine derivative (**6d**) exhibited EGFR inhibitory activity with $IC_{50}$ values of 130 and 362 nM, respectively (Table 2).

*2.2.2.2 CDK-2 inhibition assay.* Moreover, these three compounds **6o**, **6d**, and **6m** were evaluated for cyclin-dependent kinase 2 inhibitory activity.[36] The results revealed that the difluoro indolizine derivative (**6o**) revealed the most inhibitory activity against CDK-2 enzyme with an $IC_{50}$ value of 118 nM in comparison to roscovitine ($IC_{50}$ = 206 nM). Also, difluoropyrrolizine derivative (**6d**) and methylphenyl fluoroisoindolinedione derivative (**6m**) exhibited CDK-2 inhibitory activity with $IC_{50}$ values of 174 and 402 nM, respectively (Table 2). These results adhere with the anti-proliferative activity results in that the difluoro indolizine derivative **6o** was the most potent derivative against the test cell lines.

Table 2 Enzyme inhibition assay of the most active compounds against EGFR TK and CDK 2

| | EGFR inhibition | CDK-2 inhibition |
|---|---|---|
| Compound | $IC_{50}$ nM ± SE[a] | $IC_{50}$ nM ± SE[a] |
| **6d** | 362 ± 8 | 174 ± 164 |
| **6m** | 130 ± 11 | 402 ± 86 |
| **6o** | 62 ± 3 | 118 ± 16 |
| Lapatinib | 69 ± 4 | — |
| Roscovitine | — | 206 ± 10 |

[a] SE; standard error.

Table 3 P-glycoprotein expression at HepG2 cells treated with the most active compounds

| Compound | P-gp RT-PCR fold change |
|---|---|
| **6d**/HepG2 | 0.4097 |
| **6m**/HepG2 | 0.6754 |
| **6o**/HepG2 | 0.2732 |
| Tamoxifen/HepG2 | 0.2176 |
| Control HepG2 | 1 |

#### 2.2.3. Quantitative real time PCR for P-glycoprotein.

Many mechanisms are involved in cancer MDR; the most important one is ATP binding cassette (ABC) protein transporters, especially permeation protein (P-glycoprotein [P-gp]). A quantitative real-time PCR was performed to evaluate the effect of compounds **6d**, **6m**, and **6o** on P-gp in HepG-2/ADR cells (72 h) compared to tamoxifen, following the previously reported work.[12] The results presented in Table 3 showed that the three compounds caused a dose-dependent effect on P-gp, where the fluoro derivative **6o** showed a significant inhibitory effect and significant downregulation of P-gp against HepG-2 cell line by 0.2732-fold in comparison to tamoxifen with 0.2176-fold. Both compounds **6d** and **6m** showed downregulation by 0.4097 and 0.6754 folds, respectively.

#### 2.2.4. *In vitro* cytotoxicity of target compounds 6d, 6m, and 6o in drug-resistant DOX/HepG-2 cell lines.

The overexpression of P-gp in resistant cancer cells is the only observable difference between human liver cancer cells, HepG-2, and drug-resistant HepG-2 cells. *In vitro* cytotoxicity of target compounds **6d**, **6m**, and **6o** in DOX/human HepG-2 cells and their potentiation of DOX cytotoxicity were evaluated.[12,50] Compound **6m**, methylphenyl fluoroisoindolinedione derivative, displayed more potential activity ($IC_{50}$ = 3.88 μM) than its analogues difluoroindolizine, **6o** with $IC_{50}$ = 8.79 μM, and difluoropyrrolizine **6d** with $IC_{50}$ = 22.27 μM. Accordingly, the target compounds have the ability to inhibit P-gp and significantly augment the cytotoxic effect of DOX against the drug-resistant DOX/HepG-2 cancer cells, Table 4.

#### 2.2.5. Cell cycle analysis.

The cell replicates and divides through the four different phases of the cell cycle, namely G1, S

Table 4 Cytotoxic activity of the most active compounds against DOX/HepG-2 cell lines

| Compound | HepG2/ADR inhibition $IC_{50}$ μM |
|---|---|
| **6d**/Dox | 22.27 |
| **6m**/Dox | 3.88 |
| **6o**/Dox | 8.79 |

(synthesis), G2 (interphase), and M (mitosis), respectively. The impact of compound **6o** on typical cell cycle progression was assessed by flow cytometric measurement of DNA ploidy in HCT-116 cells.[51,52] Compound **6o** was applied to HCT-116 cells for 24 and 48 h at its $IC_{50}$ concentration (5.84 μM). The results confirmed that compound **6o** accumulated in the G1 and S phases (cell growth arrest at G1 and S phases) with 48.75% and 40.03%, respectively, compared to the control 42.94% and 35.77%, respectively. Thus, it may be concluded that the increased propensity for cell cycle arrest by the investigated compound led to an arrest pattern in the G1 and S phases (Fig. 6).

**2.2.6. Apoptosis analysis.** Apoptosis, or programmed cell death, is regarded as a defense mechanism against cancer spreading since it is crucial in the elimination of neoplastic cells. Malignant cells' capacity to avoid apoptosis is a defining characteristic of cancer.[53,54] Upcoming innovative anticancer agents could show their efficacy by inducing the apoptotic process through stimulation of proapoptotic molecules and inhibition of anti-apoptotic molecules. Using propidium iodide (PI) and annexin-V-FITC, flow cytometry was performed to assess the induction of apoptosis in HCT-116 cells. Following double staining with PI and annexin V-FITC (Anv), post-treatment with $IC_{50}$ of compound **6o**, and analyzed by flow cytometry, there is an increase in the total, early, and late cellular apoptosis from 2.61%, 0.52%, and 0.16% (DMSO control) to 49.16%, 15.16%, and 26.51%, respectively. These results indicate that the tested compound significantly promotes apoptosis of cancer cells (Fig. 7).

### 2.3. Molecular docking study

Molecular Operating Environment (MOE) software (version 09.2022) was used to conduct molecular modeling experiments to explore several structural possibilities regarding the potential binding mode and interactions of the most active compounds **6d**, **6m**, and **6o** into EGFR TK and CDK-2 active sites. Additionally, the EGFR kinase domain (PDB ID: 1XKK) was used to validate the docking protocol and re-dock the co-crystallized ligand quinazoline inhibitor—GW572016—into the active site.[55] On the other hand, the structure of phosphorylated

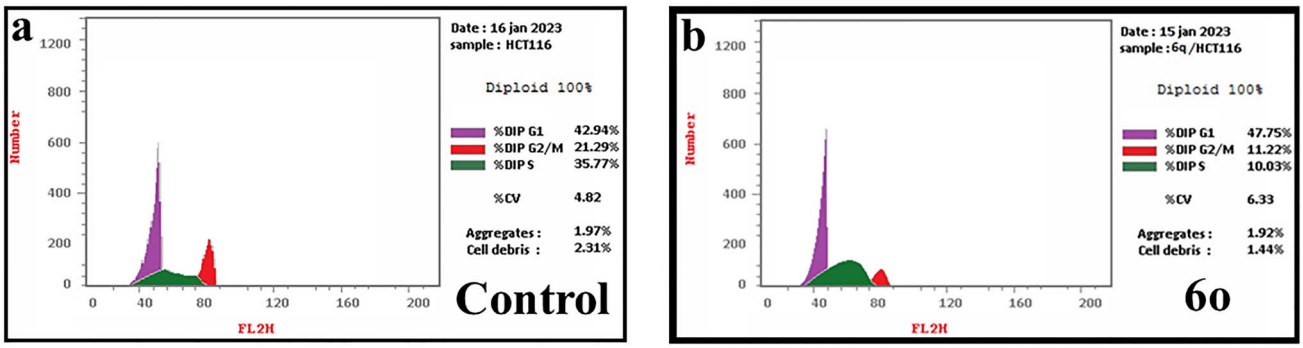


Fig. 6 Cell cycle analysis of HCT-116 cells treated with (a) DMSO as a control; (b) compound **6o**.

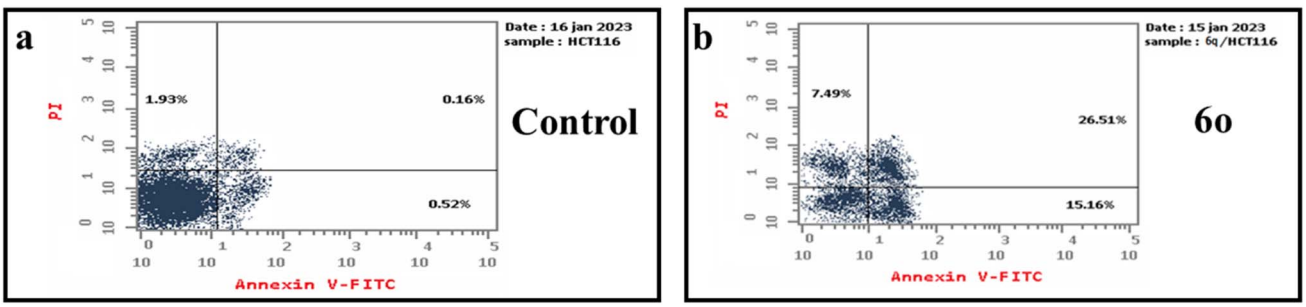


Fig. 7 Apoptosis effect in HCT-116 cancer cell line detected with annexin V-FITC/PI double staining post treatment with $IC_{50}$ of the control (a) and the tested compound **6o** (b); lower left part represents live cells, lower right part represents early/primary apoptotic cells, upper right part represents late/secondary apoptotic cells, and upper left part represents the necrotic cells.

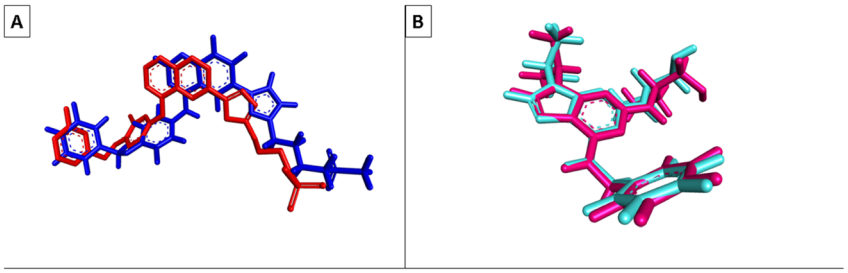


Fig. 8 (A) Superimposition of the co-crystallized (red) and re-docked ligands (blue) during validation of EGFR TK docking; (B) superimposition of the co-crystallized (purple) and re-docked ligands (cyan blue) during validation of CDK-2 docking.

Thr160 CDK-2 in complex with the inhibitor roscovitine was used to validate the docking protocol for CDK-2 (PDB ID: 3DDQ).[56] With a docking score (S) of −16.7402, the re-docked ligand displayed an rmsd of 1.6928 between the docked pose and the co-crystallized ligand for EGFR TK. When the co-crystallized ligand was docked, the rmsd between the two was 0.6221 (docking score (S) = −8.6888) for the CDK-2 enzyme (Fig. 8). Recent research revealed that the EGFR TK and CDK-2 inhibitors were positioned inside the binding site, forming intermolecular interactions with essential residues, as reported.

Lapatinib (as a positive control) and the most effective compounds **6d**, **6m**, and **6o** were docked into the EGFR's active site. The findings of the docking studies are shown in Tables 5 and 6, which also provide the type of interactions, distances (in Å) from the interacting residues, and binding affinity in kcal $mol^{-1}$. Comparing compounds **6d**, **6m**, and **6o** to co-docked ligand lapatinib as a positive control, these compounds showed strong interaction with Met793 and other essential interacting amino acids required for inhibition of EGFR TK. Notably, compound **6o** showed a strong interaction score with a binding affinity of −12.6356 kcal $mol^{-1}$ compared to lapatinib binding affinity of −13.0626 kcal $mol^{-1}$. These strong binding affinities can be explained by the numerous

Table 5 The binding energy score of the target compounds during EGFR Tk docking study

| | EGFR TK (PDB: 1XKK) | | | |
|---|---|---|---|---|
| Compound | Binding affinity (kcal $mol^{-1}$) | Distance from main residue (in Å) | | Interaction type |
| **6d** | −9.2503 | 2.54 | Met793 | Halogen bond |
| | | 3.89 | Leu718 | Hydrophobic |
| | | 4.12 | Leu844 | Hydrophobic |
| | | 3.43 | Lys745 | Hydrophobic |
| | | 2.39 | Asn842 | Hydrophobic |
| **6m** | −11.2312 | 3.34 | Met793 | H-acceptor |
| | | 4.39 | Leu718 | Hydrophobic |
| | | 4.11 | Leu844 | Hydrophobic |
| | | 3.90 | Lys745 | H-acceptor |
| | | 4.42 | Cys797 | Hydrophobic |
| **6o** | −12.6356 | 2.61 | Met793 | Halogen bond |
| | | 2.72 | Leu718 | Hydrophobic |
| | | 4.09 | Leu844 | Hydrophobic |
| | | 2.90 | Lys745 | H-acceptor |
| | | 4.15 | Cys797 | Hydrophobic |
| | | 3.51 | Arg841 | Hydrophobic |
| Lapatinib | −14.0626 | 2.96 | Met793 | H-acceptor |
| | | 4.55 | Leu718 | Hydrophobic |
| | | 3.30 | Leu844 | Hydrophobic |
| | | 4.66 | Lys745 | Hydrophobic |
| | | 3.49 | Cys775 | Halogen bond |
| | | 3.10 | Leu788 | Halogen bond |
| | | 3.13 | Thr790 | Halogen bond |
| | | 3.12 | Arg776 | Halogen bond |

Table 6 The binding energy score of the target compounds during CDK-2 docking study

| | CDK-2 (PDB: 3DDQ) | | | |
|---|---|---|---|---|
| Compound | Binding affinity (kcal $mol^{-1}$) | Distance from main residue (in Å) | | Interaction type |
| **6d** | −7.9959 | 1.98 | Leu83 | H-acceptor |
| | | 2.54 | Lys33 | Halogen bond |
| | | 2.49 | Lys89 | H-acceptor |
| | | 4.64 | Ala144 | Hydrophobic |
| | | 4.25 | Val18 | Hydrophobic |
| | | 4.61 | Leu134 | Hydrophobic |
| | | 4.19 | Ile10 | Hydrophobic |
| **6m** | −5.5006 | 2.46 | Leu83 | H-acceptor |
| | | 4.48 | Leu134 | Hydrophobic |
| | | 4.27 | Ile10 | Hydrophobic |
| | | 4.54 | Val18 | Hydrophobic |
| | | 4.61 | Phe80 | Hydrophobic |
| **6o** | −8.0611 | 2.15 | Leu83 | H-acceptor |
| | | 2.10 | Lys33 | Halogen bond |
| | | 3.35 | Glu51 | Halogen bond |
| | | 3.61 | Leu134 | Hydrophobic |
| | | 3.72 | Ala144 | Hydrophobic |
| | | 3.70 | Val18 | Hydrophobic |
| | | 3.17 | Ile10 | Hydrophobic |
| Roscovitine | −7.70482 | 2.23 | Leu83 | H-donor |
| | | 2.74 | Glu12 | H-donor |
| | | 4.24 | Ala144 | Hydrophobic |
| | | 4.01 | Ala31 | Hydrophobic |
| | | 4.44 | Lys33 | Hydrophobic |
| | | 3.79 | Val64 | Hydrophobic |
| | | 3.98 | Val18 | Hydrophobic |

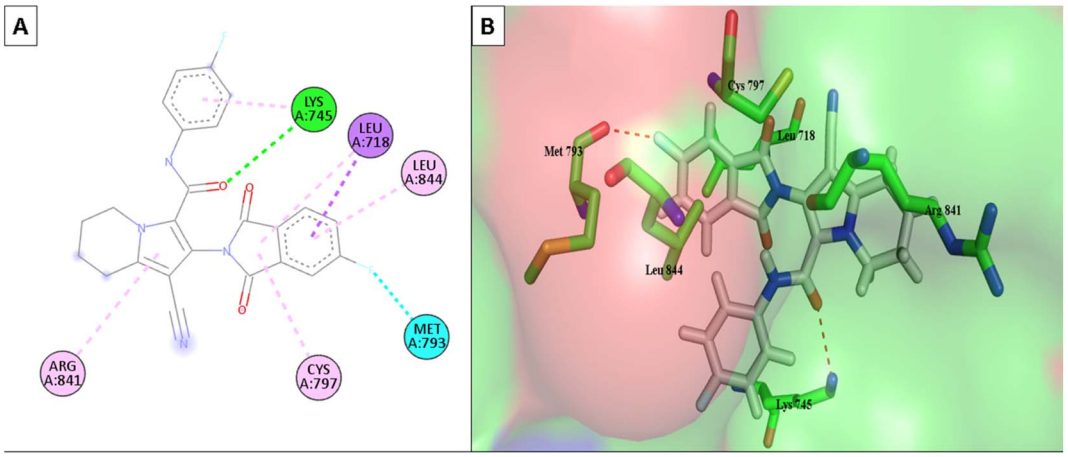


Fig. 9 (A) The 2D interaction diagram of the top docking pose of **6o** to EGFR active domain; (B) the 3D interaction diagram of the top docking pose of **6o** to EGFR active domain.

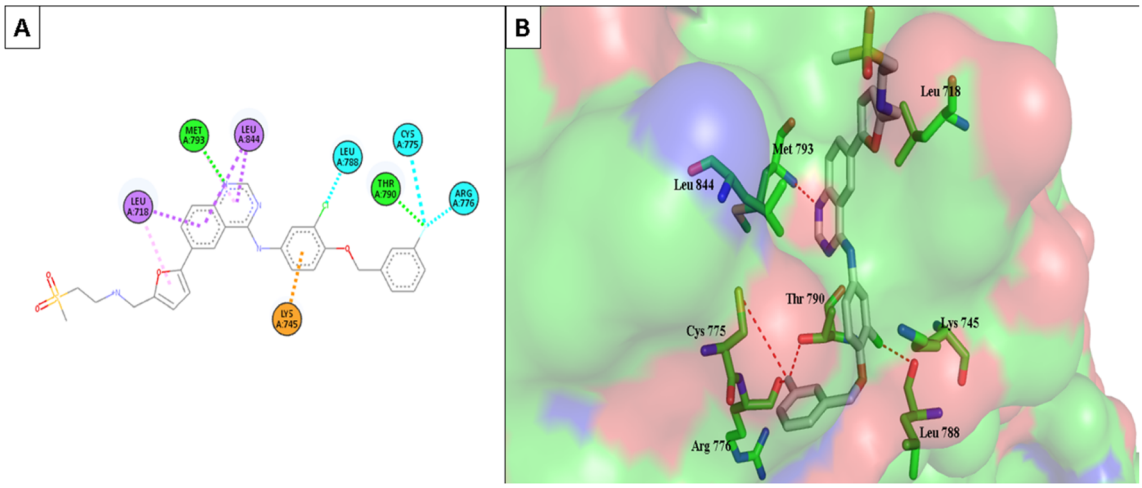


Fig. 10 (A) The 2D interaction diagram of the top docking pose of lapatinib (positive control) to EGFR active domain; (B) the 3D interaction diagram of the top docking pose of lapatinib (positive control) to EGFR active domain.

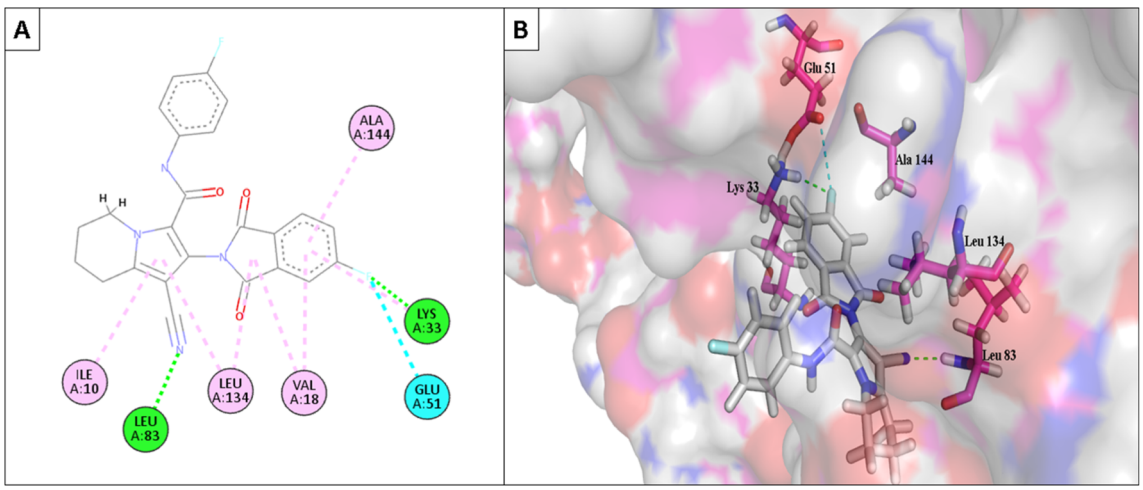


Fig. 11 (A) The 2D interaction diagram of the top docking pose of **6o** to CDK-2 active domain; (B) the 3D interaction diagram of the top docking pose of **6o** to CDK-2 active domain.

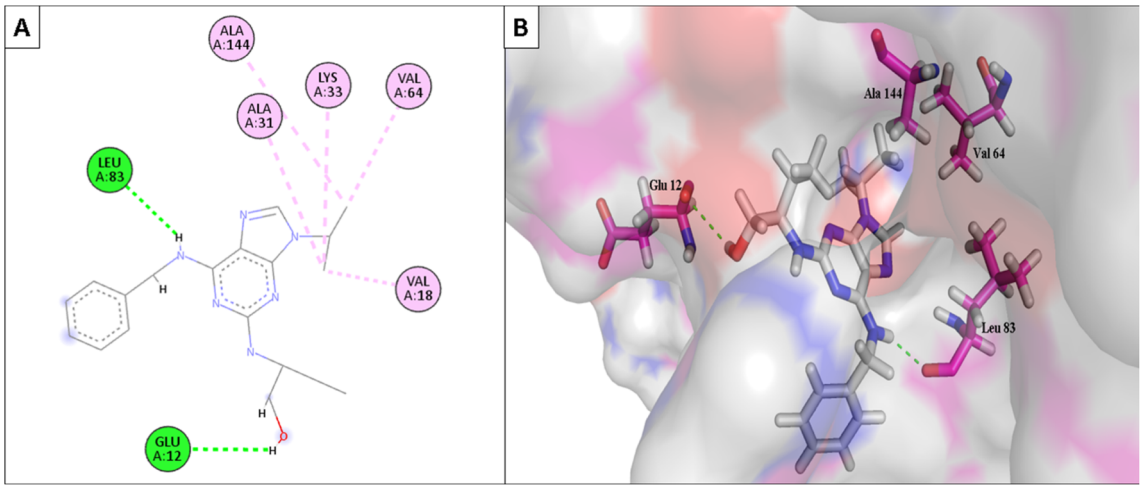


Fig. 12 (A) The 2D interaction diagram of the top docking pose of roscovitine (positive control) to CDK-2 active domain; (B) the 3D interaction diagram of the top docking pose of roscovitine (positive control) to CDK-2 active domain.

binding interactions with the key amino acid within the active site of the EGFR-TK, especially the gate-keeper Met793 and Lys 745 residues (Fig. 9 and 10).

Furthermore, the most active compounds, **6d**, **6m**, and **6o**, were docked into the CDK-2's active site along with roscovitine as a positive control. Tables 5 and 6 summarize the results of the docking study and include the type of interactions, distances (in Å) from the interacting residues, and binding affinity (in kcal $mol^{-1}$). Roscovitine, a co-docked ligand, was used as a positive control when comparing compounds **6d**, **6m**, and **6o**. These compounds demonstrated strong interactions with Leu83 and other crucial interacting amino acids necessary for CDK-2 inhibition. In particular, compounds **6d** and **6o** had a significant interaction score with a binding affinity of −7.9959 and −8.0611 kcal $mol^{-1}$, respectively, compared to Roscovitine binding affinity of −7.70482 kcal $mol^{-1}$. The strong interaction of the synthesized compound with the key amino acid with the active site of CDK-2 enzyme, mainly the –CN moiety with Leu83, was responsible for the high binding score of these compounds (Fig. 11 and 12).

Table 7 ADMET predictions for the compounds **6d**, **6m**, and **6o**

| Property | Model name | Unit | 6d | 6m | 6o |
|---|---|---|---|---|---|
| Absorption | Water solubility | Numeric (log mol $L^{-1}$) | −4.864 | −5.02 | −5.046 |
| | $Caco_2$ permeability | Numeric (log Papp in $10^{-6}$ cm $s^{-1}$) | 0.571 | 0.504 | 0.57 |
| | Intestinal absorption (human) | Numeric (% absorbed) | 95.315 | 96.201 | 96.147 |
| | P-glycoprotein substrate | Categorical (yes/no) | Yes | Yes | Yes |
| | P-glycoprotein I inhibitor | Categorical (yes/no) | Yes | Yes | Yes |
| | P-glycoprotein II inhibitor | Categorical (yes/no) | Yes | Yes | Yes |
| Distribution | Volume of distribution (human) | Numeric (log L $kg^{-1}$) | −0.193 | −0.076 | −0.138 |
| | Fraction unbound (human) | Numeric (Fu) | 0.095 | 0.054 | 0.085 |
| | BBB permeability | Numeric (log BB) | −0.614 | −0.384 | −0.592 |
| | CNS permeability | Numeric (log PS) | −2.107 | −1.856 | −2.015 |
| Metabolism | CYP2D6 substrate | Categorical (yes/no) | No | No | No |
| | CYP3A4 substrate | Categorical (yes/no) | Yes | Yes | Yes |
| | CYP1A2 inhibitor | Categorical (yes/no) | No | No | No |
| | CYP2C19 inhibitor | Categorical (yes/no) | Yes | Yes | Yes |
| | CYP2C9 inhibitor | Categorical (yes/no) | Yes | Yes | Yes |
| | CYP2D6 inhibitor | Categorical (yes/no) | No | No | No |
| | CYP3A4 inhibitor | Categorical (yes/no) | Yes | Yes | Yes |
| Excretion | Total clearance | Numeric (log mL $min^{-1}$ $kg^{-1}$) | 0.079 | −0.138 | 0.079 |
| | Renal OCT2 substrate | Categorical (yes/no) | No | No | No |
| Toxicity | AMES toxicity | Categorical (yes/no) | No | No | No |
| | Max. tolerated dose (human) | Numeric (log mg per kg per day) | −0.48 | −0.6 | −0.479 |
| | Oral rat acute toxicity ($LD_{50}$) | Numeric (mol $kg^{-1}$) | 3.091 | 3.129 | 3.141 |
| | Oral rat chronic toxicity (LOAEL) | Numeric (log mg per kg_bw per day) | 1.361 | 1.695 | 1.382 |
| | *T. pyriformis* toxicity | Numeric (log μg $L^{-1}$) | 0.395 | 0.5 | 0.39 |
| | Minnow toxicity | Numeric (log mM) | 0.411 | 0.757 | 0.294 |

Table 8 Lipinski's and Veber's violations for the compounds **6d**, **6m**, and **6o**

| Property[a] | 6d | 6m | 6o |
|---|---|---|---|
| LogP | 3.63708 | 4.1965 | 4.02718 |
| Molecular weight | 432.386 | 442.45 | 446.413 |
| NORTB[b] | 3 | 3 | 3 |
| H-bond acceptor | 5 | 5 | 5 |
| H-bond donor | 1 | 1 | 1 |
| TPSA[c] | 180.026 | 188.590 | 186.391 |

[a] The values were calculated *via* SwissADME online software.[54] [b] Number of rotatable bonds. [c] Topological polar surface area.

### 2.4. *In silico* ADMET studies

Using the PKCSM online software pkCSM (**https://biosig.lab.uq.edu.au/pkcsm/**), it was possible to estimate the physiochemical properties, pharmacokinetics, and drug-likeness profile of compounds **6d**, **6m**, and **6o**.[57,58]

The results suggested that all compounds under investigation had considerable oral absorption values. Among the analogs, compound **6d** had the highest water solubility value. It was predicted that all the assessed compounds would have high cellular permeability, particularly for intestinal cells (95.31%, 96.20%, and 96.14%) (Table 7).

It was well recognized that a molecule to be absorbed orally should obey both Lipinski and Veber'ss rules reflecting the lipophilicity–hydrophilicity equilibrium. As shown in Table 8, compounds **6d**, **6m**, and **6o** were drug-like because they adhered to Lipinski and Veber's principles.[59,60] Additionally, the determined lipophilicity was positively correlated with Caco-2 permeability but negatively correlated with the targeted compound's ability to dissolve in water. This was based on the finding that there was no correlation between drug permeability as evaluated by the human colon adenocarcinoma (Caco-2) cell line test and lipophilicity.[57]

Compound **6m** showed the most extensive BBB permeability and unbound fraction among the other analogs, according to the prediction of distribution properties. Additionally, the parameters linked to metabolism and excretion did not reveal appreciable variations among the tested molecules. Additionally, the toxicological properties of the compounds **6d**, **6m**, and **6o** were investigated. Herein, the tested compounds showed no toxicity to AMES, an *in silico* test to determine the toxicity of the synthesized compounds *via* bacterial reverse mutation assay. In addition, they showed no or minimum values for oral rat acute toxicity ($LD_{50}$) and *Tetrahymena Pyriformis* toxicity test. These results showed that the compounds **6d**, **6m**, and **6o** are predicted to be safe for human use.

## 3. Conclusion

Two new series of pyrrolizine-5-carboxamides (**6a–i**) and indolizine-6-carboxamide (**6j–q**) were designed and synthesized. IR, $^1$H NMR, $^{13}$C NMR, and mass spectroscopy confirmed the chemical structures of target compounds. Screening of the cytotoxic effect of target compounds against HePG-2, HCT-116, and MCF-7 cell lines revealed that compound **6d** was the most potent compound among its series, with $IC_{50}$ values of 7.97, 9.49, and 13.87 μM against HePG-2, HCT-116, and MCF-7, respectively. While compound **6o** exhibited the most antiproliferative activity with $IC_{50}$ values of 6.02, 5.84, and 8.89 μM against HePG-2, HCT-116, and MCF-7. EGFR and CDK-2 inhibitory effects of the most active compounds, **6d**, **6m**, and **6o**, showed that compound **6o** displayed the most inhibitory activity against EGFR with $IC_{50}$ value of 0.062 μM and CDK-2 with $IC_{50}$ value of 0.118 μM in comparison with Imatinib and Roscovitine, respectively. Annexin V-FITC apoptosis assay exposed that compound **6o** accumulated HCT-116 cells in the G1 and S phases and induced apoptosis.

## 4. Experimental

### 4.1. Chemistry

Melting points were detected by the Tomas-Hoover capillary melting apparatus without any correction. All solvents, chemicals, and reagents were supplied from Aldrich chemical company (Milwaukee, WI) and El Nasr pharmaceutical chemical companies, Cairo, Egypt. Infrared (IR) spectra were monitored as films on KBr discs using Schimadzu FT-IR 8400S spectrophotometer and values were presented as $cm^{-1}$. The purity of the synthesized compounds and the reaction progress were checked by using precoated thin layer chromatography (TLC) silica gel plates 60F254 with a thickness of 0.25 supplied from MERCK, Darmstadt, Germany. A UV lamp was used to monitor the reaction process. $^{13}$C NMR and $^1$H NMR spectra were carried out on a Bruker Avance III 400 MHz spectrophotometer, Faculty of Pharmacy, Benisuef University, Egypt, in dimethyl sulfoxide (DMSO-$d_6$) or $D_2O$ as a solvent. Chemical shift was estimated in ppm on $\delta$ scale and $J$ (Coupling constant) was estimated in Hertz. Microanalysis for C, H, and N were performed on a PerkinElmer 2400 analyzer (PerkinElmer, Norwalk, CT. USA) at the regional center for Mycology and Biotechnology, Al-Azhar University, Egypt. All results were within ±0.4% of the theoretical values.

**4.1.1. General procedure for the synthesis of 2-chloro-1*N*-[4-(un)substituted-phenyl]-acetamide (2a–f).** According to a prior report,[47] acetanilides **2a–f** were synthesized successfully. A small amount of glacial acetic acid was used to dissolve the necessary aniline (27 mmol). Dropwise additions of chloroacetyl chloride (4.55 g, 40.5 mmol) were made while the solution was continuously stirred and cooled. After chloroacetyl chloride was added, 1.5 mL of a saturated sodium acetate solution was added dropwise while stirring. Using an ice-cooled water bath, the solution was kept cool while chloroacetyl chloride was added. The resulting white precipitate was collected in a Büchner funnel, twice (2 × 30 mL) washed with water, and then recrystallized from aqueous ethanol.

**4.1.2. 2-Pyrrolidin-2-ylidene-malononitrile (4a and b).** According to the reported procedures,[48] 2-pyrrolidin-2-ylidene-malononitrile **4a and b** was synthesized. Dimethyl sulphate $(CH_3O)_2SO_2$ (3.7 g, 29.4 mmol) was stirred into a solution of 2-pyrrolidinone (2.5 g, 29.4 mmol) in dry benzene (30 mL). After being refluxed for 3 h, the reaction mixture was allowed to cool

 

to room temperature. The solution was cooled in an ice bath and made alkaline by adding sodium hydroxide drops at once (15 mol $L^{-1}$, 1.5 mL). Sodium hydroxide was added while the temperature was kept below 5 °C. After being separated, the organic phase was dried over anhydrous sodium sulphate and filtered. The benzene solution was added to malononitrile (1.25 g, 19.1 mmol) at room temperature. White crystals developed when the produced solution was swirled, and the beaker's wall was scratched. The crystals were gathered and then dried to yield 5.2 g before being recrystallized from aqueous ethanol.

**4.1.3. 6-Amino-7-cyano-*N*-[4-(un)substituted-phenyl]-2,3-dihydro-1*H*-pyrrolizine-5-carboxamide (5a–j).** Synthesis of pyrrolizine-5-carboxamides **5a–j** was obtained according to a reported method.[27] A catalytic amount of anhydrous potassium carbonate and appropriate amounts of acetanilides **2a–f** (7.5 mmol) were refluxed for 24 h with an equimolar ratio of 2-pyrrolidin-2-ylidene-malononitrile (0.5 g, 3.75 mmol) in dry acetone. Yellowish-white crystals were separated when the mixture was filtered while still hot, the flask's contents were washed twice with acetone (15 mL), and the system was allowed to cool.

*4.1.3.1 6-Amino-7-cyano-N-phenyl-2,3-dihydro-1H-pyrrolizine-5-carboxamide **5a**.* Yellow; yield 77%; mp 180–182 °C; IR: (KBr, $cm^{-1}$) 3303 (NH), 2227 (CN), 1712 (C=O); $^1$H NMR (DMSO-$d_6$, 400 MHz, $\delta$ ppm): 2.34 (m, 2H, $CH_2$), 2.91 (m, 2H, $CH_2$), 3.47 (t, 2H, $CH_2$), 6.27 (s, 2H, $NH_2$), 7.02 (t, 1H, Ar–H), 7.43 (d, 2H, $J$ = 8.9 Hz, Ar–H), 7.61 (d, 2H, $J$ = 8.9 Hz, Ar–H), 9.15 (s, 1H, NH $D_2O$ exchangeable).

*4.1.3.2 6-Amino-7-cyano-N-(p-tolyl)-2,3-dihydro-1H-pyrrolizine-5-carboxamide **5b**.* White; yield 68%; mp 232–234 °C; IR: (KBr, $cm^{-1}$) 3307 (NH), 2230 (CN), 1715 (C=O); 1H NMR (DMSO-$d_6$, 400 MHz, $\delta$ ppm): 2.23 (s, 3H, $CH_3$), 2.43 (m, 2H, $CH_2$), 2.89 (m, 2H, $CH_2$), 3.47 (t, 2H, $CH_2$), 5.56 (s, 2H, $NH_2$), 7.43 (d, 2H, $J$ = 8.9 Hz, Ar–H), 7.92 (d, 2H, $J$ = 8.9 Hz, Ar–H), 9.82 (s, 1H, NH $D_2O$ exchangeable).

*4.1.3.3 6-Amino-7-cyano-N-(4-fluorophenyl)-2,3-dihydro-1H-pyrrolizine-5-carboxamide **5c**.* Pale yellow; yield 85%; mp 271–273 °C; IR: (KBr, $cm^{-1}$) 3305 (NH), 2232 (CN), 1716 (C=O); $^1$H NMR (DMSO-$d_6$, 400 MHz, $\delta$ ppm): 2.44 (m, 2H, $CH_2$), 2.98 (m, 2H, $CH_2$), 3.67 (t, 2H, $CH_2$), 5.45 (s, 2H, $NH_2$), 7.23 (d, 2H, $J$ = 8.9 Hz, Ar–H), 7.78 (d, 2H, $J$ = 8.9 Hz, Ar–H), 9.95 (s, 1H, NH $D_2O$ exchangeable).

*4.1.3.4 6-Amino-7-cyano-N-(4-methoxyphenyl)-2,3-dihydro-1H-pyrrolizine-5-carboxamide **5d**.* Yellow; yield 84%; mp 211–213 °C; IR: (KBr, $cm^{-1}$) 3311 (NH), 2234 (CN), 1711 (C=O); $^1$H NMR (DMSO-$d_6$, 400 MHz, $\delta$ ppm): 2.20 (m, 2H, $CH_2$), 2.83 (m, 2H, $CH_2$), 3.72 (t, 2H, $CH_2$), 3.83 (s, 3H, $OCH_3$) 5.76 (s, 2H, $NH_2$), 6.99 (d, 2H, $J$ = 8.9 Hz, Ar–H), 7.60 (d, 2H, $J$ = 8.9 Hz, Ar–H), 9.23 (s, 1H, NH $D_2O$ exchangeable).

*4.1.3.5 6-Amino-N-(4-chlorophenyl)-7-cyano-2,3-dihydro-1H-pyrrolizine-5-carboxamide **5e**.* White; yield 72%; mp 238–240 °C; IR: (KBr, $cm^{-1}$) 3308 (NH), 2231 (CN), 1709 (C=O); $^1$H NMR (DMSO-$d_6$, 400 MHz, $\delta$ ppm): 2.02 (m, 2H, $CH_2$), 2.98 (m, 2H, $CH_2$), 3.78 (t, 2H, $CH_2$), 5.77 (s, 2H, $NH_2$), 7.44 (d, 2H, $J$ = 8.9 Hz, Ar–H), 7.69 (d, 2H, $J$ = 8.9 Hz, Ar–H), 9.43 (s, 1H, NH $D_2O$ exchangeable).

*4.1.3.6 6-Amino-N-(4-bromophenyl)-7-cyano-2,3-dihydro-1H-pyrrolizine-5-carboxamide **5f**.* White; yield 78%; mp 220–222 °C; IR: (KBr, $cm^{-1}$) 3313 (NH), 2227 (CN), 1714 (C=O); $^1$H NMR (DMSO-$d_6$, 400 MHz, $\delta$ ppm): 1.86 (m, 2H, $CH_2$), 3.23 (m, 2H, $CH_2$), 4.41 (t, 2H, $CH_2$), 6.24 (s, 2H, $NH_2$), 7.63 (d, 2H, $J$ = 8.9 Hz, Ar–H), 7.88 (d, 2H, $J$ = 8.9 Hz, Ar–H), 9.70 (s, 1H, NH $D_2O$ exchangeable).

*4.1.3.7 2-Amino-1-cyano-N-phenyl-5,6,7,8-tetrahydroindolizine-3-carboxamide **5g**.* Pale yellow; yield 76%; mp 214–216 °C; IR: (KBr, $cm^{-1}$) 3304 (NH), 2222 (CN), 1718 (C=O); $^1$H NMR (DMSO-$d_6$, 400 MHz, $\delta$ ppm): 1.88 (m, 2H, $CH_2$), 1.97 (m, 2H, $CH_2$), 2.75 (t, 2H, $CH_2$), 4.13 (t, 2H, $CH_2$), 5.74 (s, 2H, $NH_2$), 7.12 (t, 1H, Ar–H) 7.63 (d, 2H, $J$ = 8.9 Hz, Ar–H), 7.89 (d, 2H, $J$ = 8.9 Hz, Ar–H), 9.14 (s, 1H, NH $D_2O$ exchangeable).

*4.1.3.8 2-Amino-1-cyano-N-(p-tolyl)-5,6,7,8-tetrahydroindolizine-3-carboxamide **5h**.* Yellow; yield 84%; mp 234–236 °C; IR: (KBr, $cm^{-1}$) 3306 (NH), 2223 (CN), 1712 (C=O); $^1$H NMR (DMSO-$d_6$, 400 MHz, $\delta$ ppm): 1.75 (m, 2H, $CH_2$), 1.87 (m, 2H, $CH_2$), 2.23 (s, 3H, $CH_3$), 2.77 (t, 2H, $CH_2$), 4.31 (t, 2H, $CH_2$), 6.14 (s, 2H, $NH_2$), 7.23 (d, 2H, $J$ = 8.9 Hz, Ar–H), 7.43 (d, 2H, $J$ = 8.9 Hz, Ar–H), 9.61 (s, 1H, NH $D_2O$ exchangeable).

*4.1.3.9 2-Amino-1-cyano-N-(4-fluorophenyl)-5,6,7,8-tetrahydroindolizine-3-carboxamide **5i**.* White; yield 82%; mp 242–244 °C; IR: (KBr, $cm^{-1}$) 3301 (NH), 2224 (CN), 1706 (C=O); $^1$H NMR (DMSO-$d_6$, 400 MHz, $\delta$ ppm): 1.78 (m, 2H, $CH_2$), 1.88 (m, 2H, $CH_2$), 2.78 (t, 2H, $CH_2$), 4.11 (t, 2H, $CH_2$), 5.24 (s, 2H, $NH_2$), 7.13 (d, 2H, $J$ = 8.9 Hz, Ar–H), 7.59 (d, 2H, $J$ = 8.9 Hz, Ar–H), 9.50 (s, 1H, NH $D_2O$ exchangeable).

*4.1.3.10 2-Amino-1-cyano-N-(4-methoxyphenyl)-5,6,7,8-tetrahydroindolizine-3-carboxamide **5i**.* Yellow; yield 75%; mp 237–239 °C; IR: (KBr, $cm^{-1}$) 3305 (NH), 2346 (CN), 1772 (C=O); 1H NMR (DMSO-$d_6$, 400 MHz, $\delta$ ppm): 1.78 (m, 2H, $CH_2$), 1.87 (m, 2H, $CH_2$), 2.78 (t, 2H, $CH_2$), 3.79 (s, 3H, $OCH_3$), 4.12 (t, 2H, $CH_2$), 5.16 (s, 2H, $NH_2$), 6.90 (d, 2H, $J$ = 9.1 Hz, Ar–H), 7.50 (d, 2H, $J$ = 9.1 Hz, Ar–H), 9.35 (s, 1H, NH D2O exchangeable).

*4.1.3.11 7-Cyano-6-(1,3-dioxoisoindolin-2-yl)-N-phenyl-2,3-dihydro-1H-pyrrolizine-5-carboxamide (**6a–q**).* The phthalic anhydride (0.56 g, 3.75 mmol) was combined with the carboxamide derivatives **5a–j** (3.75 mmol) in glacial acetic acid (20 mL), which was then refluxed for 3 h. The solution was then evaporated under reduced pressure. The product was dried after being washed with water. Then, they were crystallized from a mixture of acetone/ethanol (1 : 3) to afford final compounds **6a–q**.[61]

*4.1.3.12. 7-Cyano-6-(5-fluoro-1,3-dioxoisoindolin-2-yl)-N-phenyl-2,3-dihydro-1H-pyrrolizine-5-carboxamide **6a**.* Green; yield 76%; mp 184–186 °C; IR: (KBr, $cm^{-1}$) 3302 (NH), 2233 (CN), 1720 (C=O); $^1$H NMR (DMSO-$d_6$, 400 MHz, $\delta$ ppm): 2.52 (m, 2H, $CH_2$), 3.11 (t, 2H, $CH_2$), 4.39 (t, 2H, $CH_2$), 7.08 (t, 1H, Ar–H), 7.28 (d, 2H, $J$ = 8.00 Hz, Ar–H), 7.44 (d, 2H, $J$ = 8.00 Hz, Ar–H), 7.78 (d, 1H, $J$ = 5.9 Hz, Ar–H), 7.94 (d, 1H, $J$ = 5.6 Hz, Ar–H) 8.09 (s, 1H, Ar–H) 9.97 (s, 1H, NH, $D_2O$ exchangeable), $^{13}$C NMR (100 MHz DMSO-$d_6$): $\delta$ 24.96, 25.91, 49.90, 84.63, 112.07, 112.32, 114.50, 119.78, 120.35, 121.32, 122.67, 124.54, 127.13, 127.23, 127.96, 129.03, 138.62, 146.84,157.77, 164.95, 166.18; EIMS for $C_{23}H_{15}FN_4O_3$ $m/z$ (100): 414.41 [M+] (23.98), 407.12 (100).

*4.1.3.13 7-Cyano-6-(5-fluoro-1,3-dioxoisoindolin-2-yl)-N-(p-tolyl)-2,3-dihydro-1H-pyrrolizine-5-carboxamide* ***6b***. Pale yellow; yield 73%; mp 233–235 °C; IR: (KBr, $cm^{-1}$) 3290 (NH), 2229 (CN), 1728 (C=O); $^1$H NMR (DMSO-$d_6$, 400 MHz, $\delta$ ppm): 1.92 (m, 2H, $CH_2$), 2.23 (s, 3H, $CH_3$), 3.09 (t, 2H, $CH_2$), 4.37 (t, 2H, $CH_2$), 7.06 (d, 2H, $J$ = 8.10 Hz, Ar–H), 7.30 (d, 2H, $J$ = 8.20 Hz, Ar–H), 7.67 (d, 1H, $J$ = 7.00 Ar–H), 7.92 (d, 1H, $J$ = 7.40 Hz, Ar–H) 8.07 (s, 1H, Ar–H) 9.86 (s, 1H, NH, $D_2O$ exchangeable): $\delta$ EIMS for $C_{24}H_{17}FN_4O_3$ *m*/*z* (100): 428.73 [M+] (32.72), 134.54 (100).

*4.1.3.14 7-Cyano-6-(1,3-dioxoisoindolin-2-yl)-N-(4-fluorophenyl)-2,3-dihydro-1H-pyrrolizine-5-carboxamide* ***6c***. Pale yellow; yield 67%; mp 273–275 °C; IR: (KBr, $cm^{-1}$) 3294 (NH), 2229 (CN), 1712 (C=O); $^1$H NMR (DMSO-$d_6$, 400 MHz, $\delta$ ppm): 2.51 (m, 2H, $CH_2$), 3.10 (t, 2H, $CH_2$), 4.33 (t, 2H, $CH_2$), 7.07 (d, 2H, $J$ = 8.9 Hz, Ar–H), 7.39 (d, 2H, $J$ = 8.9 Hz, Ar–H), 7.88 (t, 2H, $J$ = 6.4 Hz, Ar–H), 8.08 (d, 2H, $J$ = 8.4 Hz, Ar–H), 9.99 (s, 1H, NH $D_2O$ exchangeable), $^{13}$C NMR (100 MHz DMSO-$d_6$): $\delta$ 24.96, 25.92, 49.86, 84.66, 114.53, 115.55, 115.77, 120.06, 120.19, 123.21, 123.29, 124.31, 131.87, 135.64, 146.84, 157.81, 166.17; EIMS *m*/*z* for $C_{23}H_{15}FN_4O_3$ (100): 414.13 [M+] (29.29), 92.33 (100).

*4.1.3.15 7-Cyano-6-(5-fluoro-1,3-dioxoisoindolin-2-yl)-N-(4-fluorophenyl)-2,3-dihydro-1H-pyrrolizine-5-carboxamide* ***6d***. Yellow; yield 79%; mp 245–247 °C; IR: (KBr, $cm^{-1}$) 3298 (NH), 2233 (CN), 1720 (C=O); $^1$H NMR (DMSO-$d_6$, 400 MHz, $\delta$ ppm): 2.51 (m, 2H, $CH_2$), 3.10 (t, 2H, $CH_2$), 4.38 (t, 2H, $CH_2$), 7.11 (d, 2H, $J$ = 8.9 Hz, Ar–H), 7.44 (d, 2H, $J$ = 8.7 Hz, Ar–H), 7.75 (d, 1H, $J$ = 8.2 Hz, Ar–H), 7.94 (d, 1H, $J$ = 7.3 Hz, Ar–H), 8.09 (s, 1H, Ar–H), 10.00 (s, 1H, NH, $D_2O$ exchangeable): $\delta$ EIMS for $C_{23}H_{15}FN_4O_3$ *m*/*z* (100): 432.41 [M+] (9.67), 322.17 (100).

*4.1.3.16 7-Cyano-6-(1,3-dioxoisoindolin-2-yl)-N-(4-methoxyphenyl)-2,3-dihydro-1H-pyrrolizine-5-carboxamide* ***6e***. Yellowish white; yield 72%; mp 209–211 °C; IR: (KBr, $cm^{-1}$) 3282 (NH), 2210 (CN), 1697 (C=O); $^1$H NMR (DMSO-$d_6$, 400 MHz, $\delta$ ppm): 3.09 (m, 2H, $CH_2$), 3.71 (s, 3H, $OCH_3$), 4.10 (t, 2H, $CH_2$), 4.37 (t, 2H, $CH_2$), 6.84 (d, 2H, $J$ = 8.9 Hz, Ar–H), 7.31 (d, 2H, $J$ = 8.9 Hz, Ar–H), 7.94 (t, 2H, $J$ = 6.4 Hz, Ar–H), 8.01 (d, 2H, $J$ = 8.4 Hz, Ar–H), 9.79 (s, 1H, NH, $D_2O$ exchangeable): $\delta$ EIMS for $C_{24}H_{18}N_4O_4$ *m*/*z* (100): 426.91 [M+] (30.86), 52.23 (100).

*4.1.3.17 7-Cyano-6-(5-fluoro-1,3-dioxoisoindolin-2-yl)-N-(4-methoxyphenyl)-2,3-dihydro-1H-pyrrolizine-5-carboxamide* ***6f***. Green; yield 74%; mp 223–225 °C; IR: (KBr, $cm^{-1}$) 3286 (NH), 2229 (CN), 1728 (C=O); $^1$H NMR (DMSO-$d_6$, 400 MHz, $\delta$ ppm): 2.09 (m, 2H, $CH_2$), 3.18 (t, 2H, $CH_2$), 3.71 (s, 3H, $OCH_3$), 4.37 (t, 2H, $CH_2$), 6.85 (d, 2H, $J$ = 7.80 Hz Ar–H), 7.31 (d, 2H, $J$ = 9.10 Hz, Ar–H), 7.76 (d, 1H, $J$ = 7.30 Hz, Ar–H), 7.94 (d, 1H, $J$ = 7.60 Hz, Ar–H), 8.08 (s, 1H, Ar–H) 9.8 (s, 1H, NH, $D_2O$ exchangeable): $\delta$ EIMS for $C_{24}H_{17}FN_4O_4$ *m*/*z* (100): 444.22 [M+] (19.65), 110.32 (100).

*4.1.3.18 N-(4-Chlorophenyl)-7-cyano-6-(5-fluoro-1,3-dioxoisoindolin-2-yl)-2,3-dihydro-1H-pyrrolizine-5-carboxamide* ***6g***. Brown; yield 77%; mp 239–241 °C; IR: (KBr, $cm^{-1}$) 3296 (NH), 2233 (CN), 1720 (C=O); $^1$H NMR (DMSO-$d_6$, 400 MHz, $\delta$ ppm): 1.97 (m, 2H, $CH_2$), 3.10 (t, 2H, $CH_2$), 4.38 (t, 2H, $CH_2$), 7.33 (d, 2H, $J$ = 8.80, Ar–H), 7.47 (d, 2H, $J$ = 8.80 Hz, Ar–H), 7.79 (d, 1H, $J$ = 8.5 Hz, Ar–H),7.94 (d, 1H, $J$ = 8.7 Hz, Ar–H), 8.08 (s, 1H, Ar–H), 10.09 (s, 1H, NH, $D_2O$ exchangeable), $^{13}$C NMR (100 MHz DMSO-$d_6$): $\delta$ 24.97, 25.71, 50.02, 84.89, 87.83, 93.93, 106.64, 112.15, 118.92, 119.83, 121.33, 122.63, 122.66, 127.91, 128.16, 129.07, 129.21, 137.45, 147.04, 157.84, 165.11; EIMS for $C_{23}H_{14}ClFN_4O_3$ *m*/*z* (100): [M+], (100).

*4.1.3.19 N-(4-Bromophenyl)-7-cyano-6-(1,3-dioxoisoindolin-2-yl)-2,3-dihydro-1H-pyrrolizine-5-carboxamide* ***6h***. Yellow; yield 66%; mp 221–223 °C; IR: (KBr, $cm^{-1}$) 3329 (NH), 2233 (CN), 1732 (C=O); $^1$H NMR (DMSO-$d_6$, 400 MHz, $\delta$ ppm): 2.51 (m, 2H, $CH_2$), 3.10 (t, 2H, $CH_2$), 4.38 (t, 2H, $CH_2$), 7.41 (d, 2H, $J$ = 9.00 Hz, Ar–H), 7.46 (d, 2H, $J$ = 9.1 Hz, Ar–H), 7.94 (t, 2H, $J$ = 6.4 Hz, Ar–H), 8.00 (d, 2H, $J$ = 8.7 Hz, Ar–H), 10.09 (s, 1H, NH, $D_2O$ exchangeable), $^{13}$C NMR (100 MHz DMSO-$d_6$): $\delta$ 24.97, 25.91, 49.87, 84.71, 114.51, 116.18, 120.03, 120.23, 122.96, 124.32, 131.74, 131.88, 135.65, 138.15, 146.99, 157.88, 166.12; EIMS for $C_{23}H_{15}BrN_4O_3$ *m*/*z* (100): 475.29 [M+] (7.58), 165.26 (100).

*4.1.3.20 N-(4-Bromophenyl)-7-cyano-6-(5-fluoro-1,3-dioxoisoindolin-2-yl)-2,3-dihydro-1H-pyrrolizine-5-carboxamide* ***6i***. Brown; yield 71%; mp 234–236 °C; IR: (KBr, $cm^{-1}$) 3302 (NH), 2233 (CN), 1778 (C=O); $^1$H NMR (DMSO-$d_6$, 400 MHz, $\delta$ ppm): 2.51 (m, 2H, $CH_2$), 3.10 (t, 2H, $CH_2$), 4.38 (t, 2H, $CH_2$), 7.42 (d, 2H, $J$ = 9.00, Ar–H), 7.46 (d, 2H, $J$ = 8.80 Hz, Ar–H), 7.78 (d, 1H, $J$ = 8.2 Hz, Ar–H) 7.93 (d, 1H, $J$ = 5.40 Hz, Ar–H), 8.08 (s, 1H, Ar–H), 10.09 (s, 1H, NH, $D_2O$ exchangeable): EIMS for $C_{23}H_{14}BrFN_4O_3$ *m*/*z* (100): 493.52 [M+] (25.04), 102.19 (100).

*4.1.3.21 1-Cyano-2-(1,3-dioxoisoindolin-2-yl)-N-phenyl-5,6,7,8-tetrahydroindolizine-3-carboxamide* ***6j***. Green; yield 81%; mp 213–215 °C; IR: (KBr, $cm^{-1}$) 3302 (NH), 2225 (CN), 1708 (C=O); $^1$H NMR (DMSO-$d_6$, 400 MHz, $\delta$ ppm): 1.86 (m, 2H, $CH_2$), 1.94 (m, 2H, $CH_2$), 2.94 (t, 2H, $CH_2$), 4.19 (t, 2H, $CH_2$), 7.05 (t, 1H, Ar–H), 7.25 (t, 2H, Ar–H), 7.40 (d, 2H, $J$ = 8.7 Hz, Ar–H) 7.94 (m, 4H, Ar–H), 10.12 (s, 1H, NH, $D_2O$ exchangeable), $^{13}$C NMR (100 MHz DMSO-$d_6$): $\delta$ 19.00, 22.76, 45.92, 53.11, 88.45, 117.20, 121.19, 123.35, 124.27, 125.73, 128.99, 131.62, 136.63, 138.63, 140.80, 157.86, 166.04: EIMS for $C_{24}H_{18}N_4O_3$ *m*/*z* (100): 410.74 [M+] (12.07), 57.36 (100).

*4.1.3.22 1-Cyano-2-(5-fluoro-1,3-dioxoisoindolin-2-yl)-N-phenyl-5,6,7,8-tetrahydroindolizine-3-carboxamide* ***6k***. Pale yellow; yield 85%; mp 218–220 °C; IR: (KBr, $cm^{-1}$) 3309 (NH), 2225 (CN), 1728 (C=O); $^1$H NMR (DMSO-$d_6$, 400 MHz, $\delta$ ppm): 1.92 (m, 4H, $CH_2$, $CH_2$), 2.95 (t, 2H, $CH_2$), 4.23 (t, 2H, $CH_2$), 7.06 (t, 1H, $J$ = 6.5 Hz, Ar–H) 7.26 (d, 2H, $J$ = 8.9 Hz, Ar–H), 7.43 (d, 2H, $J$ = 11.3 Hz, Ar–H), 7.74 (d, 1H, $J$ = 8.2 Hz, Ar–H), 7.91 (d, 1H, $J$ = 7.3 Hz, Ar–H), 8.05 (s, 1H, Ar–H), 10.13 (s, 1H, NH, $D_2O$ exchangeable), $^{13}$C NMR (100 MHz DMSO-$d_6$): $\delta$ 18.92, 22.55, 45.96, 53.22, 88.41, 112.04, 112.29, 114.38, 116.96, 121.20, 122.66, 123.30, 124.51, 125.71, 127.19, 127.86, 128.99, 129.37, 138.67, 140.83, 157.79, 165.02; EIMS for $C_{24}H_{17}FN_4O_3$ *m*/*z* (100): 428.91 [M+] (9.84), 204.93 (100).

*4.1.3.23 1-Cyano-2-(1,3-dioxoisoindolin-2-yl)-N-(p-tolyl)-5,6,7,8-tetrahydroindolizine-3-carboxamide* ***6l***. Brown; yield 83%; mp 236–238 °C; IR: (KBr, $cm^{-1}$) 3313 (NH), 2222 (CN), 1716 (C=O); $^1$H NMR (DMSO-$d_6$, 400 MHz, $\delta$ ppm): 1.87 (m, 2H, $CH_2$), 2.01 (m, 2H, $CH_2$), 2.20 (s, 3H, $CH_3$), 2.98 (t, 2H, $CH_2$), 4.11 (t, 2H, $CH_2$), 7.04 (d, 2H, $J$ = 8.4 Hz, Ar–H), 7.28 (m, 4H, Ar–H), 7.95 (d, 2H, $J$ = 7.3 Hz, Ar–H) 10.02 (s, 1H, NH, $D_2O$ exchangeable): EIMS for $C_{25}H_{20}N_4O_3$ *m*/*z* (100): 424.09 [M+] (14.71), 57.36 (100).

*4.1.3.24 1-Cyano-2-(5-fluoro-1,3-dioxoisoindolin-2-yl)-N-(p-tolyl)-5,6,7,8-tetrahydroindolizine-3-carboxamide* ***6m.*** Dark brown; yield 86%; mp 242–244 °C; IR: (KBr, $cm^{-1}$) 3294 (NH), 2222 (CN), 1732 (C=O); $^1$H NMR (DMSO-$d_6$, 400 MHz, $\delta$ ppm): 1.87 (m, 2H, $CH_2$), 1.96 (m, 2H, $CH_2$), 2.23 (s, 3H, $CH_3$), 2.92 (t, 2H, $CH_2$), 4.19 (t, 2H, $CH_2$) 7.05 (d, 2H, $J$ = 7.7 Hz, Ar–H), 7.27 (d, 2H, $J$ = 8.0 Hz, Ar–H), 7.75 (d, 1H, $J$ = 8.2 Hz, Ar–H), 7.90 (d, 1H, $J$ = 7.2 Hz, Ar–H), 8.05 (s, 1H, Ar–H), 10.02 (s, 1H, NH, $D_2O$ exchangeable).

*4.1.3.25 1-Cyano-2-(1,3-dioxoisoindolin-2-yl)-N-(4-fluorophenyl)-5,6,7,8-tetrahydroindolizine-3-carboxamide* ***6n.*** Brown; yield 85%; mp 243–245 °C; IR: (KBr, $cm^{-1}$) 3303 (NH), 2225 (CN), 1708 (C=O); $^1$H NMR (DMSO-$d_6$, 400 MHz, $\delta$ ppm): 1.87 (m, 2H, $CH_2$), 1.96 (m, 2H, $CH_2$), 2.95 (t, 2H, $CH_2$), 4.21 (t, 2H, $CH_2$), 7.09 (d, 2H, $J$ = 8.8 Hz, Ar–H), 7.36 (d, 2H, $J$ = 8.8 Hz, Ar–H), 7.88 (t, 2H, $J$ = 6.8 Hz, Ar–H), 7.98 (d, 2H, $J$ = 7.5 Hz, Ar–H), 10.14 (s, 1H, NH, $D_2O$ exchangeable), $^{13}$C NMR (100 MHz DMSO-$d_6$): $\delta$ 18.91, 22.60, 45.93, 88.44, 114.41, 115.51, 115.73, 117.24, 123.08, 123.16, 124.27, 131.65, 134.98, 135.68, 140.88, 157.86, 160.19, 166.01; EIMS for $C_{24}H_{17}FN_4O_3$ $m/z$ (100): 428.67 [M+] (12.03), 195.22 (100).

*4.1.3.26 1-Cyano-2-(5-fluoro-1,3-dioxoisoindolin-2-yl)-N-(4-fluorophenyl)-5,6,7,8-tetrahydroindolizine-3-carboxamide* ***6o.*** Gray; yield 80%; mp 252–254 °C; IR: (KBr, $cm^{-1}$) 3309 (NH), 2225 (CN), 1728 (C=O); $^1$H NMR (DMSO-$d_6$, 400 MHz, $\delta$ ppm): 1.87 (m, 2H, $CH_2$), 1.96 (m, 2H, $CH_2$), 2.94 (t, 2H, $CH_2$), 4.22 (t, 2H, $CH_2$), 7.10 (d, 2H, $J$ = 8.5 Hz, Ar–H), 7.39 (d, 2H, $J$ = 8.5 Hz, Ar–H), 7.74 (d, 1H, $J$ = 8.3 Hz, Ar–H) 7.90 (d, 1H, $J$ = 7.3 Hz, Ar–H), 8.05 (s, 1H, Ar–H), 10.14 (s, 1H, NH, $D_2O$ exchangeable)$^{13}$C NMR (100 MHz DMSO-$d_6$): 18.90, 22.53, 45.96, 88.38, 112.03, 112.23, 114.36, 115.51, 115.74, 116.99, 123.01, 123.11, 123.19, 127.87, 134.94, 134.96, 140.96, 157.80, 160.21, 165.00, 165.29, 167.88; EIMS for $C_{24}H_{16}F_2N_4O_3$ $m/z$ (100): 446.52 [M+] (23.02), 339.28 (100).

*4.1.3.27 1-Cyano-2-(1,3-dioxoisoindolin-2-yl)-N-(4-methoxyphenyl)-5,6,7,8-tetrahydroindolizine-3-carboxamide* ***6p.*** Green; yield 87%; mp 227–229 °C; IR: (KBr, $cm^{-1}$) 3305 (NH), 2237 (CN), 1770 (C=O); $^1$H NMR (DMSO-$d_6$, 400 MHz, $\delta$ ppm): 1.86 (m, 2H, $CH_2$), 1.96 (m, 2H, $CH_2$), 2.98 (t, 2H, $CH_2$), 3.78 (s, 3H, $OCH_3$), 4.21 (t, 2H, $CH_2$), 6.80 (d, 2H, $J$ = 8.8 Hz, Ar–H) 7.00 (d, 2H, $J$ = 8.8 Hz, Ar–H), 7.33 (t, 2H, Ar–H), 7.95 (d, 2H, $J$ = 7.4 Hz, Ar–H) 9.93 (s, 1H, NH, $D_2O$ exchangeable): EIMS for $C_{25}H_{20}N_4O_4$ $m/z$ (100): 440.20 [M+] (9.06), 195.22 (100).

*4.1.3.28 1-Cyano-2-(5-fluoro-1,3-dioxoisoindolin-2-yl)-N-(4-methoxyphenyl)-5,6,7,8-tetrahydroindolizine-3-carboxamide* ***6q.*** Brown; yield 82%; mp 238–240 °C; IR: (KBr, $cm^{-1}$) 3306 (NH), 2345 (CN), 1770 (C=O); $^1$H NMR (DMSO-$d_6$, 400 MHz, $\delta$ ppm): 2.00 (m, 2H, $CH_2$), 2.09 (m, 2H, $CH_2$), 3.02 (t, 2H, $CH_2$), 3.78 (s, 3H, $OCH_3$), 4.17 (t, 2H, $CH_2$), 6.99 (d, 2H, $J$ = 8.8 Hz, Ar–H), 7.33 (d, 2H, $J$ = 8.80 Hz, Ar–H), 7.69 (d, 1H, $J$ = 7.9 Hz, Ar–H) 7.91 (d, 1H, $J$ = 7.2 Hz, Ar–H), 8.01 (s, 1H, Ar–H), 9.93 (s, 1H, NH, $D_2O$ exchangeable): EIMS for $C_{25}H_{19}FN_4O_4$ $m/z$ (100): 458.94 [M+] (40.95), 80.37 (100).

### 4.2. Biological activity

**4.2.1. Anti-proliferative activity.** The Holding Business for Biological Goods and Vaccines (VACSERA) in Cairo, Egypt, obtained the hepatocellular carcinoma (HEPG-2), colorectal carcinoma colon cancer (HCT-116), and mammary gland breast cancer (MCF-7) cell lines from ATCC.[49]

The aforementioned cell lines were used to examine the drug's inhibitory effects on cell growth using the MTT assay. In RPMI-1640 media with 10% foetal bovine serum, cell lines were grown. Antibiotics of 100 units per mL penicillin and 100 g $mL^{-1}$ streptomycin were introduced at 37 °C in a 5% $CO_2$ incubator. The cell lines were seeded at a density of $1.0 \times 10^4$ cells per well in a 96-well plate and incubated for 48 h at 37 °C with 5% $CO_2$.[49]

**4.2.2. Enzyme inhibition activity.** KINEXUS Corporation, Vancouver, BC, Canada, performed the assay for kinase inhibition using the radiolabeled ATP measurement technique. To assess its inhibitory effects, compounds **6d**, **6m**, and **6o** were chosen for EGFR and CDK-2 kinase inhibition activities. According to the previous report, the assay was completed. As a result, blank controls were set up, Lapatinib and Roscovitine were used as reference drugs, and the adjusted activity for protein kinase targets was obtained. $IC_{50}$ was used to display the findings.[36]

**4.2.3. Quantitative real-time PCR for P-glycoprotein.** The gene expression of P-gp was measured in HTC-116/ADR cells ($1 \times 10^5$), which were exposed to **6d**, **6o**, or **6q** (0.125, 0.250, 0.500, and 1.000 μM) for 72 h, using RT-PCR (Applied Biosystems 7500 Fast Real-Time PCR System) according to the previously reported methods.[50]

**4.2.4. *In vitro* cytotoxicity of target compounds 6d, 6m, and 6o in drug-resistant DOX/HepG-2 cell lines.** We investigated the effect of the three most active compounds, **6d**, **6o**, and **6q**, and assessed the $IC_{50}$ of DOX/HepG-2 according to the reported methods.[12]

**4.2.5. Cell cycle analysis.** 6 well plates of HCT-116 cells (1106 cells per well) were treated with $IC_{50}$ concentrations of the compound **6o**. For 30 min at 4 °C, the cells were fixed with 70% ethanol. After fixation, cells were rinsed with PBS and stained for 15 min at room temperature with no light using propidium iodide staining buffer (PI (200 g), 0.1% (v/v) Triton X-100, and 2 mg DNase-free RNase A (Sigma) in 10 mL PBS). The samples were then examined by flow cytometry utilizing the FACS Canto-II for propidium iodide-DNA fluorescence from 10 000 events (Becton Dickinson, USA).[51]

**4.2.6. Apoptosis.** Cells were transferred onto a 6-well plate and cultivated there for 18 h. The tested compound **6o** with $IC_{50}$ was applied to cells for 24 h before trypsin was used to harvest them. Before utilizing flow cytometry to assess cellular apoptosis/necrosis using the annexin V-FITC Apoptosis kit, cell pellets were washed twice with PBS (SIGMA ALDRICH). This test protocol was followed as specified by the manufacturer.[49]

*In vitro* enzyme test for cyclin-dependent kinase/cyclin 2A inhibition. The ADP-GloTM Kinase assay methodology was used for the CDK2/Cyclin2A enzyme inhibition assay. The manufacturer's instructions were followed while using the ADP-GloTM Kinase Promega Corporation test kit (2800 Woods Hollow Road, Madison, WI 53711–5399, USA). ADP-GloTM reagent was introduced to the CDK2 reaction after it had finished using ATP and producing ADP in order to stop the kinase process and exhaust any remaining ATP. ADP was afterwards transformed to

ATP using the kinase detection reagent, and the recently formed ATP was then used to produce light *via* a luciferase reaction. DMSO was applied as a solvent for the investigated compound, which was introduced to the mixture at various quantities during the assay, which was carried out at room temperature. On the Tecan-spark READER, continuous kinetic monitoring of enzyme activity was finished. The enzyme inhibition percentages of all the compounds at each concentration were calculated, and Graphpad was used to get the $IC_{50}$ values.[36]

### 4.3. Molecular docking study

Using MOE 2022.09.01 (Molecular Operating Environment, Chemical Computing Group, Canada) software, docking studies, investigations, and calculations were performed for the molecular modeling of EGFR TK (PDB ID: 1XKK) and CDK-2 (PDB ID: 3DDQ).[55,56]

After docking by placement utilizing the Triangle Matcher protocol and post-placement refinement using Rigid Receptor in the case of EGFR TK docking, poses for docked compounds were scored by the initial and final rescoring methodologies (London dG). After docking by placement using the Triangle Matcher procedure, poses for docked compounds were scored using the initial rescoring methodology (London dG) and the final rescoring methodology (GBVI/WSA dG), and post-placement refinement was Rigid Receptor in the case of the CDK-2 study. A combination of Discovery Studio Client Visualizer 2021 and Pymol 2.5 was used to generate 2D and 3D captions.[49,62,63]

### 4.4. *In silico* ADMET studies

The molecular structures of the synthesized pyrrolizine and indolizine derivatives **6d**, **6m**, and **6o** were uploaded into the ADME/Tox web tools SwissADME and pkCSM-pharmacokinetics using the simplified molecular-input line-entry specification (SMILES) nomenclature. To depict the ADME/Tox profile, we picked the key ADME/Tox attributes from the available web resources.

## Conflicts of interest

There are no conflicts to declare.

## References

1 M. C. Hulvat, Cancer incidence and trends, *Surgical Clinics*, 2020, **100**(3), 469–481.
2 S. T. Pan, *et al.*, Molecular mechanisms for tumour resistance to chemotherapy, *Clin. Exp. Pharmacol. Physiol.*, 2016, **43**(8), 723–737.
3 A.-M. Florea and D. Büsselberg, Cisplatin as an anti-tumor drug: cellular mechanisms of activity, drug resistance and induced side effects, *Cancers*, 2011, **3**(1), 1351–1371.
4 Q. Wu, *et al.*, Multi-drug resistance in cancer chemotherapeutics: mechanisms and lab approaches, *Cancer Lett.*, 2014, **347**(2), 159–166.
5 C. M. Neophytou, *et al.*, Apoptosis deregulation and the development of cancer multi-drug resistance, *Cancers*, 2021, **13**(17), 4363.
6 Q. Gao, *et al.*, Opportunities and challenges for co-delivery nanomedicines based on combination of phytochemicals with chemotherapeutic drugs in cancer treatment, *Adv. Drug Delivery Rev.*, 2022, 114445.
7 R. van der Meel, *et al.*, Smart cancer nanomedicine, *Nat. Nanotechnol.*, 2019, **14**(11), 1007–1017.
8 Z. Chen, *et al.*, Mammalian drug efflux transporters of the ATP binding cassette (ABC) family in multidrug resistance: A review of the past decade, *Cancer Lett.*, 2016, **370**(1), 153–164.
9 A. Lazarowski, ABC-transporters and drug efflux in hematologic cancers, in *Drug Efflux Pumps in Cancer Resistance Pathways: From Molecular Recognition and Characterization to Possible Inhibition Strategies in Chemotherapy*, Elsevier, 2020, pp. 149–195.
10 J. Veiga-Matos, F. Remião and A. Motales, Pharmacokinetics and toxicokinetics roles of membrane transporters at kidney level, *J. Pharm. Pharm. Sci.*, 2020, **23**, 333–356.
11 X. Gu, *et al.*, Synthesis and biological evaluation of bifendate–chalcone hybrids as a new class of potential P-glycoprotein inhibitors, *Bioorg. Med. Chem.*, 2012, **20**(8), 2540–2548.
12 A. M. Shawky, *et al.*, Discovery of new pyrimidopyrrolizine/indolizine-based derivatives as P-glycoprotein inhibitors: Design, synthesis, cytotoxicity, and MDR reversal activities, *Eur. J. Med. Chem.*, 2021, **218**, 113403.
13 B. Wang, *et al.*, Exploration of 1, 2, 3-triazole-pyrimidine hybrids as potent reversal agents against ABCB1-mediated multidrug resistance, *Eur. J. Med. Chem.*, 2018, **143**, 1535–1542.
14 A. Tan, *et al.*, Evaluation of cytotoxic potentials of some isoindole-1, 3-dione derivatives on HeLa, C6 and A549 cancer cell lines, *Med. Chem.*, 2020, **16**(1), 69–77.
15 D. Berger, *et al.*, Novel multidrug resistance reversal agents, *J. Med. Chem.*, 1999, **42**(12), 2145–2161.
16 M. Labbozzetta, *et al.*, Novel insights on [1, 2] oxazolo [5, 4-e] isoindoles on multidrug resistant acute myeloid leukemia cell line, *Drug Dev. Res.*, 2022, **83**(6), 1331–1341.
17 J. Tamariz, *et al.*, *Pyrrolizidine alkaloids*, The alkaloids: chemistry and biology, 2018, vol. 80, pp. 1–314.
18 X. Wei, W. Ruan and K. Vrieling, Current knowledge and perspectives of pyrrolizidine alkaloids in pharmacological applications: A mini-review, *Molecules*, 2021, **26**(7), 1970.
19 A. M. Gouda, *et al.*, Design, synthesis and pharmacological evaluation of novel pyrrolizine derivatives as potential anticancer agents, *Bioorg. Chem.*, 2014, **53**, 1–7.
20 S. Tavolari, *et al.*, Licofelone, a dual COX/5-LOX inhibitor, induces apoptosis in HCA-7 colon cancer cells through the mitochondrial pathway independently from its ability to affect the arachidonic acid cascade, *Carcinogenesis*, 2008, **29**(2), 371–380.
21 W. Liu, *et al.*, Investigations on cytotoxicity and anti-inflammatory potency of licofelone derivatives, *Eur. J. Med. Chem.*, 2011, **46**(3), 907–913.

22 A. M. Gouda, *et al.*, Antitumor activity of pyrrolizines and their Cu (II) complexes: Design, synthesis and cytotoxic screening with potential apoptosis-inducing activity, *Eur. J. Med. Chem.*, 2018, **145**, 350–359.
23 V. Lisowski, *et al.*, Design, synthesis and antiproliferative activity of tripentones: a new series of antitubulin agents, *Bioorg. Med. Chem. Lett.*, 2001, **11**(16), 2205–2208.
24 C. Rochais, *et al.*, MR22388, a novel anti-cancer agent with a strong FLT-3 ITD kinase affinity, *Cancer Lett.*, 2013, **331**(1), 92–98.
25 A. M. Gouda, *et al.*, Pyrrolizines: design, synthesis, anticancer evaluation and investigation of the potential mechanism of action, *Bioorg. Med. Chem.*, 2017, **25**(20), 5637–5651.
26 B. C. Q. Nguyen, *et al.*, 1, 2, 3-Triazolyl ester of Ketorolac: A "Click Chemistry"-based highly potent PAK1-blocking cancer-killer, *Eur. J. Med. Chem.*, 2017, **126**, 270–276.
27 M. A. Abourehab, *et al.*, Pyrrolizine/indolizine-cinnamaldehyde Schiff bases: Design, synthesis, biological evaluation, ADME, and molecular docking study, *Eur. J. Med. Chem. Rep.*, 2022, **4**, 100036.
28 C. Lima, S. F. Eto and M. Lopes-Ferreira, Shedding Light on the Drug–Target Prediction of the Anti-Inflammatory Peptide Tn P with Bioinformatics Tools, *Pharmaceuticals*, 2022, **15**(8), 994.
29 L. H. Al-Wahaibi, *et al.*, Synthesis and Biological Evaluation of Indole-2-Carboxamides with Potent Apoptotic Antiproliferative Activity as EGFR/CDK2 Dual Inhibitors, *Pharmaceuticals*, 2022, **15**(8), 1006.
30 M. A. Mansour, *et al.*, Insights into fourth generation selective inhibitors of (C797S) EGFR mutation combating non-small cell lung cancer resistance: a critical review, *RSC Adv.*, 2023, **13**(27), 18825–18853.
31 A. Belal, Synthesis, molecular docking and antitumor activity of novel pyrrolizines with potential as EGFR-TK inhibitors, *Bioorg. Chem.*, 2015, **59**, 124–129.
32 Y. Wang, *et al.*, Design, synthesis and biological evaluation of pyrimidine derivatives as novel CDK2 inhibitors that induce apoptosis and cell cycle arrest in breast cancer cells, *Bioorg. Med. Chem.*, 2018, **26**(12), 3491–3501.
33 T. Otto and P. Sicinski, Cell cycle proteins as promising targets in cancer therapy, *Nat. Rev. Cancer*, 2017, **17**(2), 93–115.
34 H. A. Abd El-wahab, *et al.*, New cell cycle checkpoint pathways regulators with 2-Oxo-indoline scaffold as potential anticancer agents: Design, synthesis, biological activities and *in silico* studies, *Bioorg. Chem.*, 2022, **120**, 105622.
35 A. M. Shawky, *et al.*, Pharmacophore-based virtual screening, synthesis, biological evaluation, and molecular docking study of novel pyrrolizines bearing urea/thiourea moieties with potential cytotoxicity and CDK inhibitory activities, *J. Enzyme Inhib. Med. Chem.*, 2021, **36**(1), 15–33.
36 A. Belal, *et al.*, Design, synthesis and molecular docking of new fused 1 H-pyrroles, pyrrolo [3, 2-d] pyrimidines and pyrrolo [3, 2-e][1, 4] diazepine derivatives as potent EGFR/CDK2 inhibitors, *J. Enzyme Inhib. Med. Chem.*, 2022, **37**(1), 1884–1902.
37 X.-J. Liu, *et al.*, Recent development of multi-target VEGFR-2 inhibitors for the cancer therapy, *Bioorg. Chem.*, 2023, 106425.
38 J. Tang and T. Aittokallio, Network pharmacology strategies toward multi-target anticancer therapies: from computational models to experimental design principles, *Curr. Pharm. Des.*, 2014, **20**(1), 23–36.
39 I. Shawish, *et al.*, Pyrazolyl-s-triazine with indole motif as a novel of epidermal growth factor receptor/cyclin-dependent kinase 2 dual inhibitors, *Front. Chem.*, 2022, **10**, 1078163.
40 M. S. Altowyan, *et al.*, Synthesis, characterization, and cytotoxicity of new spirooxindoles engrafted furan structural motif as a potential anticancer agent, *ACS Omega*, 2022, **7**(40), 35743–35754.
41 H. A. Gomaa, *et al.*, Optimization and SAR investigation of novel 2, 3-dihydropyrazino [1, 2-a] indole-1, 4-dione derivatives as EGFR and BRAFV600E dual inhibitors with potent antiproliferative and antioxidant activities, *Bioorg. Chem.*, 2022, **120**, 105616.
42 M. H. Saad, *et al.*, Discovery of new symmetrical and asymmetrical nitrile-containing 1, 4-dihydropyridine derivatives as dual kinases and P-glycoprotein inhibitors: synthesis, *in vitro* assays, and *in silico* studies, *J. Enzyme Inhib. Med. Chem.*, 2022, **37**(1), 2489–2511.
43 W. S. Hamama, *et al.*, Recent advances in the chemistry of 2-chloroquinoline-3-carbaldehyde and related analogs, *RSC Adv.*, 2018, **8**(16), 8484–8515.
44 M. A. Metwally and E. Abdel-Latif, Thiohydantoins: synthetic strategies and chemical reactions, *J. Sulfur Chem.*, 2012, **33**(2), 229–257.
45 S. Kumari, S. Paliwal and R. Chauhan, Synthesis of pyrazole derivatives possessing anticancer activity: Current status, *Synth. Commun.*, 2014, **44**(11), 1521–1578.
46 E. Abdel-Latif, M. M. Fahad and M. A. Ismail, Synthesis of N-aryl 2-chloroacetamides and their chemical reactivity towards various types of nucleophiles, *Synth. Commun.*, 2020, **50**(3), 289–314.
47 D. Kumar, *et al.*, *Synthesis and antimicrobial investigation of some novel phenyl pyrazole, azetidinone and diazenyl ethanone derivatives of benzofurans*, 2008.
48 K. M. Attalah, *et al.*, Ethyl benzoate bearing pyrrolizine/indolizine moieties: Design, synthesis and biological evaluation of anti-inflammatory and cytotoxic activities, *Bioorg. Chem.*, 2020, **94**, 103371.
49 A. M. Shaker, *et al.*, Novel 1, 3-diaryl pyrazole derivatives bearing methylsulfonyl moiety: Design, synthesis, molecular docking and dynamics, with dual activities as anti-inflammatory and anticancer agents through selectively targeting COX-2, *Bioorg. Chem.*, 2022, **129**, 106143.
50 L. Sun, *et al.*, Icaritin reverses multidrug resistance of HepG2/ADR human hepatoma cells *via* downregulation of MDR1 and P-glycoprotein expression, *Mol. Med. Rep.*, 2013, **8**(6), 1883–1887.

51 H. S. Mohamed, *et al.*, Design, synthesis, biological assessment, and in-silico studies of 1, 2, 4-triazolo [1, 5-a] pyrimidine derivatives as tubulin polymerization inhibitors, *Bioorg. Chem.*, 2022, **121**, 105687.

52 A. F. Zaher, *et al.*, Synthesis, antitumor screening and cell cycle analysis of novel benzothieno [3, 2-b] pyran derivatives, *J. Enzyme Inhib. Med. Chem.*, 2016, **31**(sup4), 145–153.

53 B. Xie, *et al.*, Synthesis, characterization and anticancer efficacy studies of iridium (III) polypyridyl complexes against colon cancer HCT116 cells, *Molecules*, 2022, **27**(17), 5434.

54 I. A. Abdel-Azziz, *et al.*, Design, synthesis and mechanistic studies of benzophenones hydrazone derivatives as cathepsin inhibitors, *J. Mol. Struct.*, 2023, **1274**, 134583.

55 M. A. Abourehab, *et al.*, Globally approved EGFR inhibitors: Insights into their syntheses, target kinases, biological activities, receptor interactions, and metabolism, *Molecules*, 2021, **26**(21), 6677.

56 K. H. Oudah, *et al.*, Design, synthesis and molecular docking of novel pyrazolo [1, 5-a][1, 3, 5] triazine derivatives as CDK2 inhibitors, *Bioorg. Chem.*, 2019, **92**, 103239.

57 M. A. Mansour, A. M. AboulMagd and H. M. Abdel-Rahman, Quinazoline-Schiff base conjugates: *in silico* study and ADMET predictions as multi-target inhibitors of coronavirus (SARS-CoV-2) proteins, *RSC Adv.*, 2020, **10**(56), 34033–34045.

58 D. E. Pires, T. L. Blundell and D. B. Ascher, pkCSM: predicting small-molecule pharmacokinetic and toxicity properties using graph-based signatures, *J. Med. Chem.*, 2015, **58**(9), 4066–4072.

59 C. A. Lipinski, *et al.*, Experimental and computational approaches to estimate solubility and permeability in drug discovery and development settings, *Adv. Drug Delivery Rev.*, 1997, **23**(1–3), 3–25.

60 T. Hou, *et al.*, ADME evaluation in drug discovery. 6. Can oral bioavailability in humans be effectively predicted by simple molecular property-based rules?, *J. Chem. Inf. Model.*, 2007, **47**(2), 460–463.

61 S. E. Abbas, *et al.*, Novel substituted and fused pyrrolizine derivatives: Synthesis, anti-inflammatory and ulcerogenecity studies, *Eur. J. Med. Chem.*, 2010, **45**(2), 482–491.

62 S. S. El-Hawary, *et al.*, Characterization of Promising Cytotoxic Metabolites from Tabebuia guayacan Hemsl.: Computational Prediction and *In Vitro* Testing, *Plants*, 2022, **11**(7), 888.

63 Y. O. Mekhlef, A. M. AboulMagd and A. M. Gouda, Design, Synthesis, Molecular docking, and biological evaluation of novel 2, 3-diaryl-1, 3-thiazolidine-4-one derivatives as potential anti-inflammatory and cytotoxic agents, *Bioorg. Chem.*, 2023, **133**, 106411.